Electronic Supplementary Material (ESI) for Physical Chemistry Chemical Physics.

Supplementary information:

A structural investigation of ionic liquid mixtures

Richard P. Matthews,[#,1] *Ignacio J. Villar-Garcia,*[#,1,2] *Cameron C. Weber,*[#,1] *Jeraime Griffith, Fiona Cameron,*[1] *Jason P. Hallett,*[1,3] *Patricia A. Hunt,*[1] *Tom Welton**[,1]

[1] Department of Chemistry, Imperial College London, London, SW7 2AZ, UK.

[2] Department of Materials, Imperial College London, London, SW7 2AZ, UK.

[3] Department of Chemical Engineering, Imperial College London, London, SW7 2AZ, UK.

[#] These authors contributed equally to this work

Section A: Experimental

General Procedures

Unless otherwise specified, syntheses were performed using standard Schlenk techniques or within a glovebox under a dry nitrogen atmosphere. Reagents purchased were of the highest purity available and dried from appropriate drying agents.

Dichloromethane-*d*$_2$ NMR Experiments

The required quantity of IL was weighed into a screw cap vial within an inert atmosphere glovebox. CD_2Cl_2 (0.75 mL) was added to the vial and accurately weighed. The homogeneous solution was transferred to a 5 mm NMR tube which was capped then sealed with parafilm. ^1H and ^{13}C NMR experiments were conducted on a Bruker 400 MHz NMR fitted with an autosampler with the temperature maintained at 25 °C. Spectra were referenced to the residual solvent peak (δ_H= 5.32 ppm, δ_C = 54.00 ppm).

NMR of Undiluted Ionic Liquid Mixtures

A sample of each IL was added to a 5 mm NMR tube, a flame sealed capillary of DMSO-*d*$_6$ inserted as a lock and chemical shift reference (δ_H = 2.50, δ_C = 39.51) and the tube capped and sealed with parafilm. ^1H and ^{13}C NMR spectra were obtained on a Bruker 500 MHz NMR spectrometer with the temperature maintained at 80 °C. Chemical shifts were fitted to the modified equation originally introduced by Bosch and Rosés as well as Skwierczynski and Connors for the preferential solvation of dyes, depicted in Equation 2,[1, 2] using the Origin data analysis package.

Synthesis of Ionic Liquids

1-Butyl-3-methylimidazolium chloride ([C_4C_1im]Cl). 1-methylimidazole (160.33 g, 1.95 mol) in ethyl acetate (200 mL) and 1-chlorobutane (250 mL, 2.38 mol) were combined and stirred at 60 °C for 19 days leading to the formation of a biphasic mixture. The resultant solution was cooled to −20 °C for 16 h resulting in the formation of a white crystalline solid. The solid was filtered and washed with ethyl acetate (2 × 50 mL). The solid was then dissolved in hot acetonitrile and enough ethyl acetate added to produce a phase separation. The resultant solution was cooled to −20 °C for 16 h yielding [C_4C_1im]Cl as a white crystalline solid which was filtered and dried *in vacuo* (313.41 g, 1.79 mol, 91.9%).

^1H NMR δ (ppm) (400 MHz, acetone-*d*$_6$) 10.86 (s, 1H, NC*H*N), 7.96 (m, 1H, NC*H*CHN), 7.89 (m, 1H, NCHC*H*N), 4.45 (t, $^3J_{HH}$ = 7 Hz, 2H, NCH_2), 4.10 (s, 3H, NCH_3), 1.92 (m, 2H, NCH_2CH_2), 1.36 (m, 2H, CH_2CH_3), 0.94 (t, $^3J_{HH}$ = 7 Hz, 3H, CH_2CH_3). $^{13}C\{^1H\}$ NMR δ (ppm) (101 MHz, acetone-*d*$_6$) 139.52 (s, N*C*HN), 124.38 (s, N*C*HCHN), 123.14 (s, NCH*C*HN), 49.81 (s, NCH_2), 36.42 (s, NCH_3), 32.98 (s, NCH_2CH_2), 20.05 (s, CH_2CH_3), 13.83 (s, CH_2CH_3).

1-Butyl-3-methylimidazolium bromide ([C_4C_1im]Br). 1-methylimidazole (103 g, 1.25 mol) was transferred into a dry 1L two-neck round-bottomed flask with stirring bar. Ethyl acetate (100 mL) was added, the mixture stirred and 1-bromobutane (181 g, 1.32 mol) added dropwise. The mixture was stirred at room temperature overnight then the temperature was raised to 35°C and the emulsion stirred for 4 days. The flask was cooled to −20°C in order to crystallise the [C_4C_1im]Br. The product was recrystallised from acetonitrile and the white crystals were dried *in vacuo* and stored under a dry nitrogen atmosphere.

^{1}H NMR δ (ppm) (400 MHz, DMSO-*d*$_6$): 9.23 (s, 1H, NC*H*N), 7.80 (s, 1H, NC*H*CHN), 7.73 (s, 1H, NCHC*H*N), 4.17 (t, 2H, NC*H*$_2$), 3.86 (s, 3H, NC*H*$_3$), 1.76 (m, 2H, NCH$_2$C*H*$_2$), 1.25 (m, 2H, C*H*$_2$CH$_3$), 0.90 (t, 3H, CH$_2$C*H*$_3$). ^{13}C NMR δ (ppm) (101 MHz, DMSO-*d*$_6$): 136.51 (s, N*C*HN), 123.55 (s, N*C*HCHN), 122.25 (s, NCH*C*HN), 48.41 (s, N*C*H$_2$), 35.76 (s, N*C*H$_3$), 31.33 (s, NCH$_2$*C*H$_2$), 18.74 (s, *C*H$_2$CH$_3$), 13.27 (s, CH$_2$*C*H$_3$).

1-Butyl-3-methylimidazolium dimethylphosphate ([C$_4$C$_1$im][Me$_2$PO$_4$]). 1-Butylimidazole (49.26 g, 0.397 mol) was dissolved in acetonitrile (50 mL) and trimethylphosphate (50 mL, 0.427) added dropwise. The resultant solution was heated with stirring to 60 °C for 84 h, the solvent removed and the resultant viscous liquid washed with ethyl acetate (5 × 150 mL) then dried at 50 °C *in vacuo* to afford [C$_4$C$_1$im][Me$_2$PO$_4$] as a viscous pale yellow liquid (87.66 g, 0.332 mol, 83.6%).

^{1}H NMR *δ* (ppm) (400 MHz, acetone-*d*$_6$) 10.65 (s, 1H, NC*H*N), 7.92 (m, 1H, NC*H*CHN), 7.85 (m, 1H, NCHC*H*N), 4.38 (t, $^3J_{\mathrm{HH}}$ = 7 Hz, 2H, NC*H*$_2$), 4.10 (s, 3H, NC*H*$_3$), 3.14 (d, $^3J_{\mathrm{HP}}$ = 10 Hz, C*H*$_3$OP), 1.89 (m, 2H, NCH$_2$C*H*$_2$), 1.35 (m, 2H, C*H*$_2$CH$_3$), 0.93 (t, $^3J_{\mathrm{HH}}$ = 7 Hz, 3H, CH$_2$C*H*$_3$). ^{13}C NMR *δ* (ppm) (101 MHz, acetone-*d*$_6$) 140.41 (s, N*C*HN), 124.49 (s, N*C*HCHN), 123.23 (s, NCH*C*HN), 52.04 (d, $^2J_{\mathrm{CP}}$ = 6 Hz, *C*H$_3$OP) 49.75 (s, N*C*H$_2$), 36.28 (s, N*C*H$_3$), 33.07 (s, NCH$_2$*C*H$_2$), 20.08 (s, *C*H$_2$CH$_3$), 13.85 (s, CH$_2$*C*H$_3$). ^{31}P{^{1}H} NMR *δ* (ppm) (162 MHz, acetone-*d*$_6$) 1.93 (s, CH$_3$O*P*).

1-Butyl-3-methylimidazolium *bis*(trifluoromethanesulfonyl)imide ([C$_4$C$_1$im][NTf$_2$]). In air, [C$_4$C$_1$Im]Cl (79.92 g, 0.458 mol) and lithium *bis*(trifluoromethanesulfonyl)imide (140.63 g, 0.490 mol) were dissolved separately in water (150 mL for both). These aqueous solutions were combined resulting in the immediate formation of a second phase. Dichloromethane (200 mL) was added to increase the volume of the lower phase and the resultant organic phase separated and washed with water until the aqueous phase tested negative for halide using a 0.1 M AgNO$_3$ solution (4 × 150 mL). The dichloromethane solvent was removed and the resultant liquid dried at 50 °C *in vacuo* to yield [C$_4$C$_1$im][NTf$_2$] as a colourless liquid (187.64 g, 0.447 mol, 97.7%).

^{1}H NMR *δ* (ppm) (400 MHz, acetone-*d*$_6$) 9.00 (s, 1H, NC*H*N), 7.76 (m, 1H, NC*H*CHN), 7.70 (m, 1H, NCHC*H*N), 4.36 (t, $^3J_{\mathrm{HH}}$ = 7 Hz, 2H, NC*H*$_2$), 4.05 (s, 3H, NC*H*$_3$), 1.92 (m, 2H, NCH$_2$C*H*$_2$), 1.38 (m, 2H, C*H*$_2$CH$_3$), 0.94 (t, $^3J_{\mathrm{HH}}$ = 7 Hz, 3H, CH$_2$C*H*$_3$). ^{13}C{^{1}H} NMR *δ* (ppm) (101 MHz, acetone-*d*$_6$) 137.43 (s, N*C*HN), 124.87 (s, N*C*HCHN), 123.48 (s, NCH*C*HN), 121.04 (q, $^1J_{\mathrm{CF}}$ = 320 Hz, *C*F$_3$), 50.31 (s, N*C*H$_2$), 36.71 (s, N*C*H$_3$), 32.78 (s, NCH$_2$*C*H$_2$), 20.00 (s, *C*H$_2$CH$_3$), 13.67 (s, CH$_2$*C*H$_3$). ^{19}F{^{1}H} NMR *δ* (ppm) (376 MHz, acetone-*d*$_6$) −79.96 (s, C*F*$_3$).

1-Butyl-3-methylimidazolium trifluoromethanesulfonate ([C$_4$C$_1$im][OTf]). [C$_4$C$_1$im]Cl (108.30 g, 0.620 mol) was dissolved in dichloromethane (300 mL). This solution was added to a stirred slurry of lithium trifluoromethanesulfonate (105.09 g, 0.674 mol) in dichloromethane (300 mL) and the resultant slurry stirred at room temperature for 60 h. The slurry was filtered and the dichloromethane phase washed successively with water until the aqueous phase tested negative for halide using a 0.1 M AgNO$_3$ solution (14 × 5 mL). The dichloromethane was then removed and the resultant liquid dried at 50 °C *in vacuo* to afford [C$_4$C$_1$im][OTf] as a colourless liquid (151.21 g, 0.525 mol, 84.6%).

^{1}H NMR *δ* (ppm) (400 MHz, acetone-*d*$_6$) 9.10 (s, 1H, NC*H*N), 7.78 (m, 1H, NC*H*CHN), 7.71 (m, 1H, NCHC*H*N), 4.35 (t, $^3J_{\mathrm{HH}}$ = 7 Hz, 2H, NC*H*$_2$), 4.04 (s, 3H, NC*H*$_3$), 1.91 (m, 2H, NCH$_2$C*H*$_2$), 1.37 (m, 2H, C*H*$_2$CH$_3$), 0.93 (t, $^3J_{\mathrm{HH}}$ = 7 Hz, 3H, CH$_2$C*H*$_3$). ^{13}C{^{1}H} NMR *δ* (ppm) (101 MHz, acetone-*d*$_6$) 137.74 (s, N*C*HN), 124.79 (s, N*C*HCHN), 123.44 (s, NCH*C*HN), 122.30 (q, $^1J_{\mathrm{CF}}$ = 320 Hz, *C*F$_3$), 50.19 (s, N*C*H$_2$), 36.63 (s, N*C*H$_3$), 32.80 (s, NCH$_2$*C*H$_2$), 20.00 (s, *C*H$_2$CH$_3$), 13.71 (s, CH$_2$*C*H$_3$). ^{19}F{^{1}H} NMR *δ* (ppm) (376 MHz, acetone-*d*$_6$) 79.00 (s, C*F*$_3$).

1-Butyl-3-methylimidazolium thiocyanate ($[C_4C_1im][SCN]$). $[C_4C_1im]Cl$ (2.09 g, 12.0 mmol) in acetonitrile (15 mL) was combined with barium thiocyanate (1.84 g, 6.00 mmol) in acetonitrile (15 mL) and the solution stirred for 4 h, during which time a white precipitate formed. The liquid phase was isolated by centrifugation and the solvent removed to yield $[C_4C_1Im][SCN]$ as a slightly pink liquid (1.86 g, 9.43 mmol, 79%).

^{1}H NMR δ (ppm) (400 MHz, DMSO-*d₆*) 9.30 (s, 1H, NC*H*N), 7.82 (m, 1H, NC*H*CHN), 7.75 (m, 1H, NCHC*H*N), 4.19 (t, $^3J_{HH}$ = 7.2 Hz, 2H, NCH_2), 3.87 (s, 3H, NCH_3), 1.77 (m, 2H, NCH_2CH_2), 1.27 (m, 2H, CH_2CH_3), 0.90 (t, $^3J_{HH}$ = 7.2 Hz, 3H, CH_2CH_3). $^{13}C\{^1H\}$ NMR δ (ppm) (101 MHz, $CDCl_3$) 136.67 (s, N*C*HN), 131.66 (s, SCN), 123.85 (s, N*C*HCHN), 122.30 (s, NCH*C*HN), 50.11 (s, NCH_2), 36.78 (s, NCH_3), 32.09 (s, NCH_2CH_2), 19.52 (s, CH_2CH_3), 13.48 (s, CH_2CH_3). *m/z* ($LSIMS^+$) 139 ($[C_4C_1im]$, 100%), ($LSIMS^-$) 26 (CN^-, 95%), 32 (S^-, 94%), 58 (SCN^-, 100%).

1-Butyl-3-methylimidazolium acetate ($[C_4C_1im][OAc]$). $[C_4C_1im]Br$ (130.2 g, 0.594 mol) and dry silver acetate (99.7 g, 0.597 mol) were transferred into a 500 ml conical flask. The flask was covered with aluminium foil to prevent the photodegradation of silver salts. Distilled water (250 mL) was added and the suspension stirred overnight. The yellowish precipitate was filtered off and the filtrate tested for the presence of silver and bromide: one or two drops of the solution were diluted with 0.5 mL distilled water in a sample vial and one or two drops of test solution were added. The test solutions were dilute HCl for silver ions and 1M $AgNO_3$ for bromide. Aqueous $[C_4C_1im]Br$ was added dropwise if excess silver was observed and silver acetate if excess bromide. A sample was taken after each drop and then tested again. The addition was stopped when the tests for bromide and silver ions were negative. The solution was placed in the continuous extractor and extracted with ethyl acetate for 16 hours. The water was removed with the rotary evaporator. $[C_4C_1im][OAc]$ was dried to completion using high vacuum at 60°C.

^{1}H NMR δ (ppm) (400 MHz, DMSO-*d₆*): 10.71 (s, 1H, NC*H*N), 7.91 (s, 1H, NC*H*CHN), 7.83 (s, 1H, NCHC*H*N), 4.20 (t, 2H, NCH_2), 3.88 (s, 3H, NCH_3), 1.75 (m, 2H, NCH_2CH_2), 1.58 (s, 3H, CH_3CO_2), 1.22 (m, 2H, CH_2CH_3), 0.87 (t, 3H, CH_2CH_3). ^{13}C NMR δ (ppm) (101 MHz, DMSO-*d₆*): 173.59 (s, CH_3CO_2), 137.04 (s, N*C*HN), 124.02 (s, N*C*HCHN), 122.27 (s, NCH*C*HN), 48.41 (s, NCH_2), 35.76 (s, NCH_3), 31.33 (s, NCH_2CH_2), 18.74 (s, CH_2CH_3), 13.27 (s, CH_2CH_3). *m/z* (Fab+): 139 ($[C_4C_1im]^+$, 100%), 337 ($([C_4C_1im]_2[OAc])^+$, 14%). *m/z* (Fab-): 59 ($[OAc]^-$, 100%), 119 ($(H[OAc]_2)^-$, 61%) 257 ($[C_4C_1im][OAc]_2)^-$, 68%), 455 ($([C_4C_1im]_2[OAc]_3)^-$, 28%).

1-Butyl-1-methypyrrolidinium chloride ($[C_4C_1pyrr]Cl$). 1-chlorobutane (67.76 g, 0.73 mol) was added dropwise under N_2, to a mixture of 1-methylpyrrolidine (57.60 g, 0.68 mol) in acetonitrile (50 mL). The mixture was heated at 75 °C for 36 hours. The solution was cooled to room temperature then further cooled to 4 °C for 1 day. The acetonitrile was decanted, leaving a white solid. The white solid was washed with ethyl acetate and dried *in vacuo* for 24 hours, affording $[C_4C_1pyrr]Cl$ as a white crystalline solid (93.66 g, 0.53 mol, 77.9% yield).

^{1}H NMR δ (ppm) (400 MHz, DMSO-*d₆*): 3.49 (6H, m, ring (CH_2)N(CH_2) and chain NCH_2CH_2), 3.02 (3H, s, NCH_3), 2.05 (4H, s, ring NCH_2CH_2), 1.65 (2H, m, NCH_2CH_2), 1.27 (2H, m, CH_2CH_3), 0.89 (3H, t, J = 8 Hz, CH_2CH_3). $^{13}C\{^1H\}$ NMR δ(ppm) (101 MHz, DMSO-*d₆*): 63.14 (s, ring (CH_2)N(CH_2)), 62.51 (s, chain NCH_2CH_2), 47.25 (s, NCH_3), 24.95 (s, ring NCH_2CH_2), 20.97 (s, chain NCH_2CH_2), 19.29 (s, CH_2CH_3), 13.51 (s, CH_2CH_3) *m/z* (ESI+): 142 ($[C_4C_1pyrr]^+$, 100%), 319 ($[C_4C_1pyrr]_2Cl)^+$ *m/z* (FAB-): 35 (Cl^-, 10%), 212 ($([C_4C_1pyrr]Cl_2)^-$, 40%) MP: 124 °C Elemental analysis (calc): %C = 60.70 (60.83), %H = 11.20 (11.34), %N = 7.94 (7.88)

1-Butyl-1-methypyrrolidinium *bis*(trifluoromethanesulfonyl)imide ($[C_4C_1pyrr][NTf_2]$). To a flask containing a stirred solution of $[C_4C_1pyrr]Cl$ (34.0 g, 0.191 mol) in dichloromethane (50 mL) was added lithium *bis*(trifluoromethanesulfonyl)imide under N_2 (54.94 g, 0.191 mol). The mixture was stirred for 24 h and the white precipitate was allowed to settle. Cannula filtration and subsequent washing of the sodium chloride residue with dichloromethane (2 × 50 mL) gave a colourless liquid, which was further diluted with dichloromethane (100 mL) and washed with aliquots of water until halide free, as indicated by the $AgNO_3$ test of the water washings. The liquid was dried *in vacuo* for 3 h at 50 °C then filtered through a short pad (1−1.5 cm) of acidic and then basic alumina and thoroughly dried *in vacuo* at 50°C for a further 8 h to afford $[C_4C_1pyrr][NTf_2]$ (61.23 g, 0.145 mol, 75.9% yield) as a colourless liquid.

^1H NMR δ (ppm) (500 MHz, DMSO-d_6 in capillary): 2.94 (4H, m, ring CH_2NCH_2), 2.74 (2H, m, NCH_2CH_2), 2.44 (s, 3H, NCH_3), 1.63 (4H, m, ring NCH_2CH_2), 1.19 (2H, m, $NCH_2CH_2CH_2$), 0.82 (2H, m, CH_2CH_3), 0.40 (t, $^3J_{HH}$ = 7.4 Hz, 3H, CH_2CH_3). $^{13}C\{^1H\}$ NMR δ (ppm) (126 MHz, DMSO-d_6 in capillary): 118.86 (q, $^1J_{CF}$ = 320 Hz, CF_3), 63.07 (s, ring CH_2NCH_2), 63.02 (s, ring NCH_2CH_2), 46.69 (s, NCH_3), 24.18 (s, $NCH_2CH_2CH_2$), 20.04 (s, $NCH_2CH_2CH_2$), 18.14 (s, CH_2CH_3), 11.56 (s, CH_2CH_3). *m/z* (ESI+): 142 ($[C_4C_1pyrr]^+$, 45%), 564 (($[C_4C_1pyrr]_2[NTf_2])^+$, 100%) *m/z* (ESI-): 280 ($[NTf_2]^-$, 100%), 702 (($[C_4C_1pyrr][NTf_2]_2)^-$, 10%) Elemental analysis (calc): C 31.38% (31.28%), H 4.69% (4.77%), N 6.55% (6.63%).

Section B: Computational Procedures

DFT calculations using Becke's three-parameter exchange functional[3] in combination with the Lee, Yang and Parr correlation functional[4] (B3LYP) have been carried out with a 6–311+G(d,p) basis set as implemented in the Gaussian 09 (revision D.01) suite of programs.[5] Grimme's (-D3)[6, 7] dispersion correction with the Becke and Johnson damping (BJ-damping) function[8-10] has been added to the B3LYP functional (B3LYP-D3BJ) to account for dispersion interactions. Further details of the computational details have been reported elsewhere.[11]

$[C_1C_1im]_2[Me_2PO_4]_2$ IP-dimer structures were generated from the corresponding $[C_1C_1im]_2Cl_2$ structures by replacing the Cl^- anions with $[Me_2PO_4]^-$ anions. These were arranged such that non-alkylated oxygen atoms were orientated so as to maximise the H-bonding with the imidazolium ring H-atoms. This was followed by a two-step optimisation procedure; 1) the cation atoms were frozen and a partial optimisation (only anion positions optimised) has been performed, 2) release of all nuclei to allow a full optimisation. Subsequently minima have been confirmed via vibrational analysis.

The IP-dimer names have been partitioned into four components as described previously.[11] First, the parent part of the name is taken from the general motif, i.e. middle (M) or diagonal (D). The second and third sections are based on the relative positions of the anions in relation to cation 1 and cation 2, respectively, i.e. front (F), side (S), back (B), top (T) or bottom (Bt). The final component details the relative $[C_1C_1im]^+$ cation ring orientations, i.e. parallel (P), rotated (R), antiparallel (A) or T-shape (T). For example, the M_FS_SF_A IP-dimer structure is found as the lowest energy conformer for the Cl^-. This structure has a middle (M) arrangement of ions, and exhibits alternate front and side (FS) H-bonding interactions between a cation and both anions. Moreover, the $[C_1C_1im]^+$ cation rings are stacked in an antiparallel rotated orientation (A). Hence, M_FS_SF_A refers to a middle conformation with the rings anti-parallel, M_FS_SF_R refers to the rings being rotated, see Fig. 12.

To incorporate the effect of a solvent environment CPCM (dichloromethane) and SMD ($[C_4C_1im]Cl$ IL) calculations have been performed. These were started from the gas-phase geometries and re-optimised using the same optimisation criteria as above. Confirmation of minima has also been carried out via vibrational analysis. SMD calculations have been carried out using macroscopic solvent descriptors for $[C_4C_1im]Cl$ as described by Bernales et al.[12] These descriptors include static dielectric constant, the index of refraction, the macroscopic surface tension, Abraham's hydrogen bond acidity and basicity parameters for the solvent when treated as a solute, fraction of non-hydrogen atoms that are aromatic carbon atoms, and the fraction of non-hydrogen atoms that are electronegative halogen atoms. As there is no generally accepted static dielectric established for $[C_4C_1im]Cl$ this has been estimated at 11.5 (the average for 10 ILs as presented by Bernales et al.). All other parameter values have been sourced from experimental papers.[13, 14] NMR calculations have been carried out at the B3LYP/6-311+G(2d,p)//B3LYP-D3BJ/6-311+G(d,p) level using the Gauge-Independent Atomic Orbital (GIAO) method as implemented in the Gaussian software. Analysis of the electron density within the QTAIM framework has been carried out using the AIMALL software package.[15]

Table S1. Conformer energies (kJ mol^{-1}) for the $[C_1C_1im]_2Cl_2$ and $[C_1C_1im]_2[Me_2PO_4]_2$ IPD, in the gas-phase, CPCM calculations employing CH_2Cl_2 solvent and IL ($[C_4C_1im]Cl$) SMD model.

	$[C_1C_1im]_2Cl_2$			gas phase	$[C_1C_1im]_2[Me_2PO_4]_2$			gas phase
	gas-phase	CH_2Cl_2	IL	N…N	gas-phase	CH_2Cl_2	IL	N…C
	ΔE	ΔE	ΔE	(Å)	ΔE	ΔE	ΔE	(Å)
front-IP	2.35	0.00	0.00		-	0.00	0.72	
side-IP	37.30	9.83	7.37		-	12.19	8.53	
top-IP	0.00	8.33	8.06		0.00	2.37	0.00	
M_FS_SF_R	0.00	0.00	0.00	3.509	16.36	4.97	0.00	3.469
M_FS_SF_A	0.67	5.06	9.13	3.525	19.52	6.77	3.77	3.543
D_FT_TF_A	3.26	-	-	5.583	0.00	0.00	0.02	5.232

Table S2. $\rho_{BCP}(r)$ evaluated for the H-bond interactions in the IP-dimers of $[C_1C_1im]_2Cl_2$ and $[C_1C_1im]_2[Me_2PO_4]_2$ and the ^{13}C NMR chemical shifts evaluated relative to the front conformer.

	gas phase			CH_2Cl_2			IL	
	H^2	$H^{4/5}$	δC^2	δC^4	δC^5	δC^2	δC^4	δC^5
	$\rho_{BCP}(r)$ au	$\rho_{BCP}(r)$ au	ppm	ppm	ppm	ppm	ppm	ppm
$[C_1C_1im]_2[Me_2PO_4]_2$								
stacked M_FS_SF_A	0.036	0.022	−1.60	+2.95	-0.23	-1.20	+4.15	0.00
stacked M_FS_SF_R			**-3.25**	**+3.74**	**-1.19**	**-1.40**	**+4.33**	**-2.59**
alternating D_FT_TF_A	0.035	0.008	+0.06	-0.36	-0.08	+0.42	+1.02	-0.66
$[C_1C_1im]_2Cl_2$								
stacked M_FS_SF_A	0.022	0.014	−1.79	+2.84	-1.12	-1.73	+3.32	-1.67
stacked M_FS_SF_R			**-2.36**	**+2.25**	**-0.96**	**-1.48**	**+2.13**	**-1.24**
alternating D_FT_TF_A	0.024	-	-	-	-	-	-	-

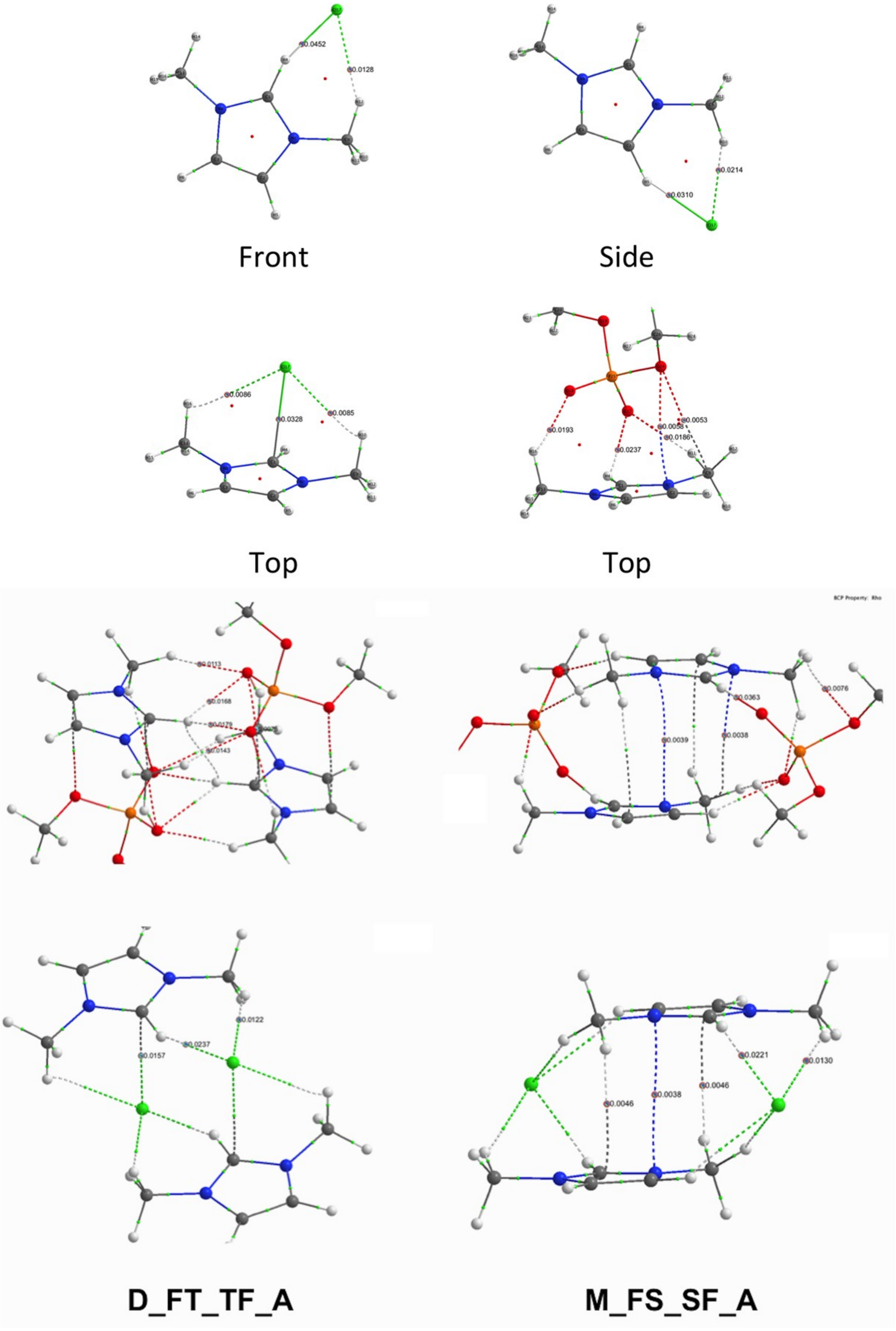

Fig. S1 Representative QTAIM topological maps for the ion-pair and IP-dimer structures for selected $[C_1C_1im]_2Cl_2$ and $[C_1C_1im]_2[Me_2PO_4]_2$ IP-dimers. Topological maps only show BCPs (green) and corresponding bond paths. The electron density ρ for selected BCPs are shown.

Table S3. NMR chemical shifts relative to TMS (ppm) for the $[C_1C_1im]_2Cl_2$ and $[C_1C_1im]_2[Me_2PO_4]_2$ IP-dimers, employing a CPCM CH_2Cl_2 solvent model.

		$[C_1C_1im]_2Cl_2$			$[C_1C_1im]_2[Me_2PO_4]_2$	
	C^2	C^4	C^5	C^2	C^4	C^5
front IP	148.0	132.1	131.2	151.1	132.2	130.9
M_FS_SF_A	146.2	134.9	130.1	149.5	135.2	130.7
M_FS_SF_R	145.6	134.3	130.2	147.8	135.9	129.7
D_FT_TF_A		Not a stable structure		151.2	131.8	130.8

Table S4. NMR chemical shifts relative to DMSO (ppm) for the $[C_1C_1im]_2Cl_2$ and $[C_1C_1im]_2[Me_2PO_4]_2$ IP-dimers, employing a SMD IL ($[C_4C_1im]Cl$) solvent model.

		$[C_1C_1im]_2Cl_2$			$[C_1C_1im]_2[Me_2PO_4]_2$	
	C^2	C^4	C^5	C^2	C^4	C^5
front IP	99.4	83.2	83.3	101.2	83.8	82.7
M_FS_SF_A	97.7	86.6	81.6	100.0	87.9	82.7
M_FS_SF_R	97.9	85.4	82.0	99.8	88.1	80.2
D_FT_TF_A		Not a stable structure		101.6	84.8	82.1

Molecular dynamics (MD) simulation runs have been performed for pure and mixed ILs using the DL_POLY classic (version_2.19) simulation code.[16] Seven different mixed IL compositions have been simulated for each of the $[C_4C_1im]Cl_x[OTf]_{1-x}$ and $[C_4C_1im][Me_2PO_4]_x[NTf_2]_{1-x}$ systems at 400K, X = {0.0, 0.109, 0.195, 0.305,0.500,0.805, 1.0}. This temperature is significantly higher than the melting points of the pure systems; 340 K for $[C_4C_1im]Cl$, 290 K for $[C_4C_1im][OTf]$, <298 K for $[C_4C_1im][Me_2PO_4]$ and 270 K for $[C_4C_1im][NTf_2]$.

Inter- and intra-molecular interactions for the $[C_4C_1im]^+$, Cl^-, [OTf] and $[NTf_2]^-$ ions have been taken from the potential model developed by Canongia Lopes and Padua (CL&P), taking into account corrections made by the authors in the supporting information of a later publication.[17, 18] The $[Me_2PO_4]^-$ potential has been taken from the OPLS-AA force field.[19] These parameters have been previously found to perform adequately when combined with the CL&P force field.[20, 21]

All simulations have been carried out using 256 cation and anion ion-pairs. Initial configurations were generated by placing the ions randomly in a cubic box using the Packmol software package,[22] followed by equilibration at a higher temperature and then controlled cooling. Additional 5ns runs in the isothermal-isobaric (NPT) ensemble have been carried out. Final densities and box lengths are reported in Table S6. NPT simulations were followed by 5 ns equilibration and 20 ns production runs in the canonical (NVT) ensemble. Data used for analysis has been collected from the 20 ns production runs only. Periodic boundary conditions have been applied and the equations of motion have been integrated using a leapfrog-type Verlet algorithm[23] with the time step set to 1 fs. A Nose-Hoover thermostat has been used to constrain the temperature (relaxation time of 0.1 ps).[24] The pressure was fixed to be one atmosphere in all constant pressure simulations (relaxation time of 0.5 ps) with isotropic volume fluctuations. A modified version of the SHAKE algorithm has been employed to constrain intra-molecular C-H bonds.[25, 26] A cut-off radius of 16.0 Å has been applied for all Lennard-Jones (LJ) interactions and long-range corrections have been taken into account. Moreover, the Ewald summation technique has been used to account for the long-range electrostatic interactions.[23]

Cation-anion and cation-cation site-site pair radial distribution functions (RDFs), angular distribution functions (ADF) and spatial distribution functions (SDF) have been evaluated using the TRAVIS program.[27] In addition, ADFs have been computed up to the first minimum of the corresponding H–X and C–X RDFs and SDFs have been generated using VMD.[28]

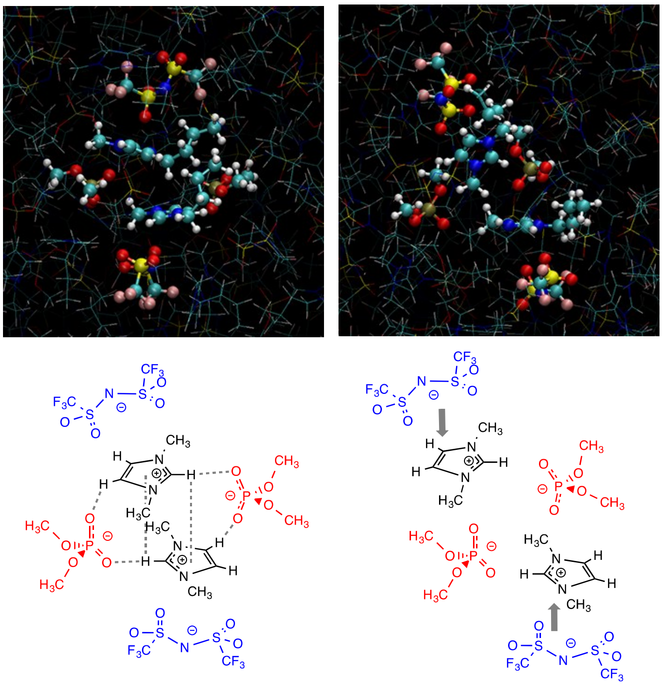

Fig. S2 Snapshots from MD simulations and cartoons representing the arrangement of ions within the $[C_4C_1im][Me_2PO_4]_{0.50}[NTf_2]_{0.50}$ mixture (a) shows stronger π^+-π^+ stacking and H-bonding with Me_2PO_4 and (b) shows stronger anion-π^+ interactions.

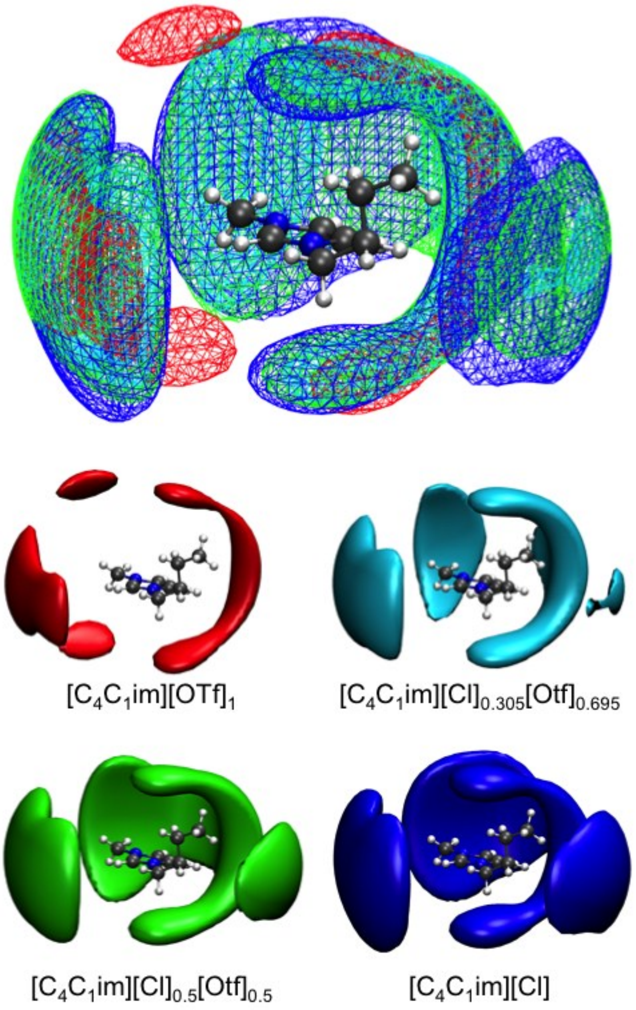

$[C_4C_1im][OTf]_1$ $[C_4C_1im][Cl]_{0.305}[Otf]_{0.695}$

$[C_4C_1im][Cl]_{0.5}[Otf]_{0.5}$ $[C_4C_1im][Cl]$

Fig. S3 Overlap (top) and individual (below) cation-cation SDFs at several concentrations for the $[C_4C_1im]Cl_x[OTf]_{1-x}$ mixtures. All isosurfaces are shown at 1.5 times bulk.

The large surfaces at the rear of the imidazolium ring for both Cl^- and $[OTf]^-$ (Fig. S3) show that there is essentially no preferential interaction at this site, consistent with the $\Delta G \approx 0.0$ kJ mol^{-1} obtained from the K values from the model based on the experimental NMR data.

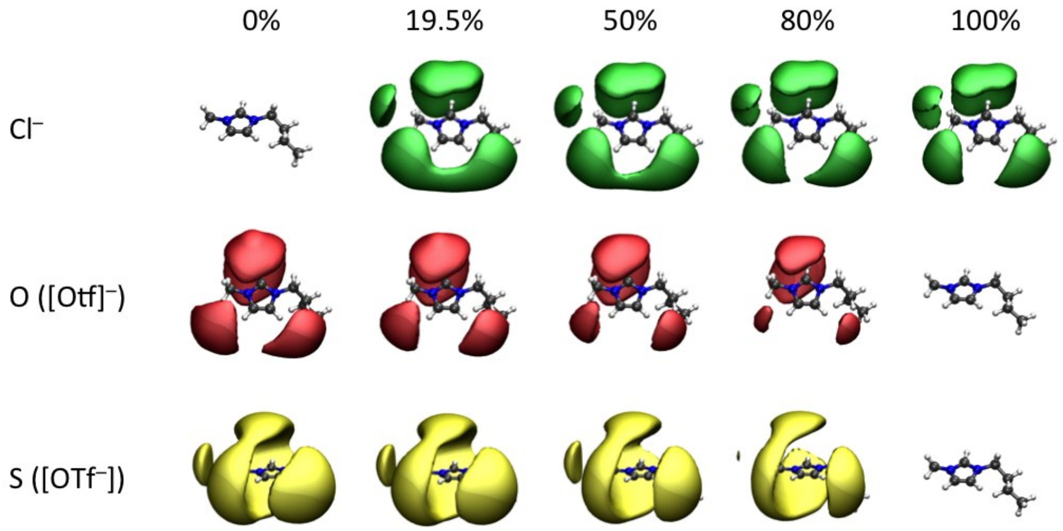

Fig. S4 Spatial density maps of selected atoms (anions) around the cation for several Cl⁻ concentrations in the $[C_4C_1im]Cl_x[OTf]_{1-x}$ mixtures. Isosurfaces: Cl in green, O ($[OTf]^-$) in red and S ($[OTf]^-$) in yellow. Isosurfaces are shown at 2.5 times the normalised atomic density.

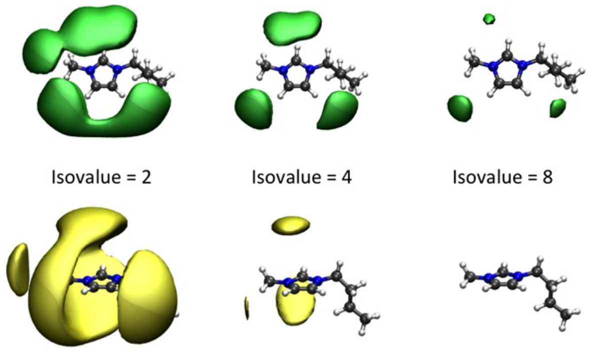

Fig. S5 Spatial density maps for the $[C_4C_1im]Cl_{0.50}[OTf]_{0.50}$ mixture.

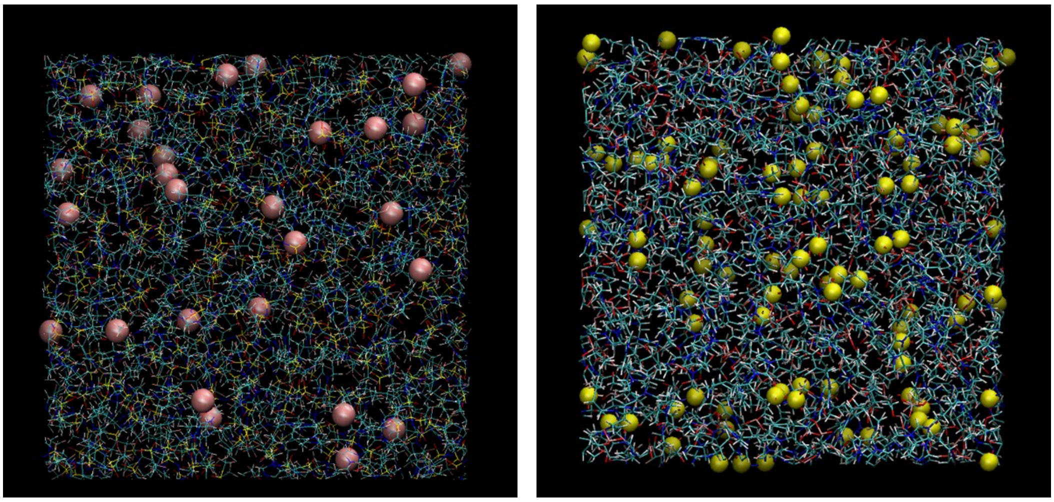

Fig. S6 Snap shot of a single trajectory frame showing the even distribution of the anions within the solution for the $[C_4C_1im][Me_2PO_4]_x[NTf_2]_{1-x}$ mixture. Ions are represented as stick structures, (a) x=0.2 Phosphorus atoms shown as pink spheres, (b) x=0.8 sulfur atoms shown as yellow spheres (there are 2 sulfur atoms per $[NTf_2]^-$).

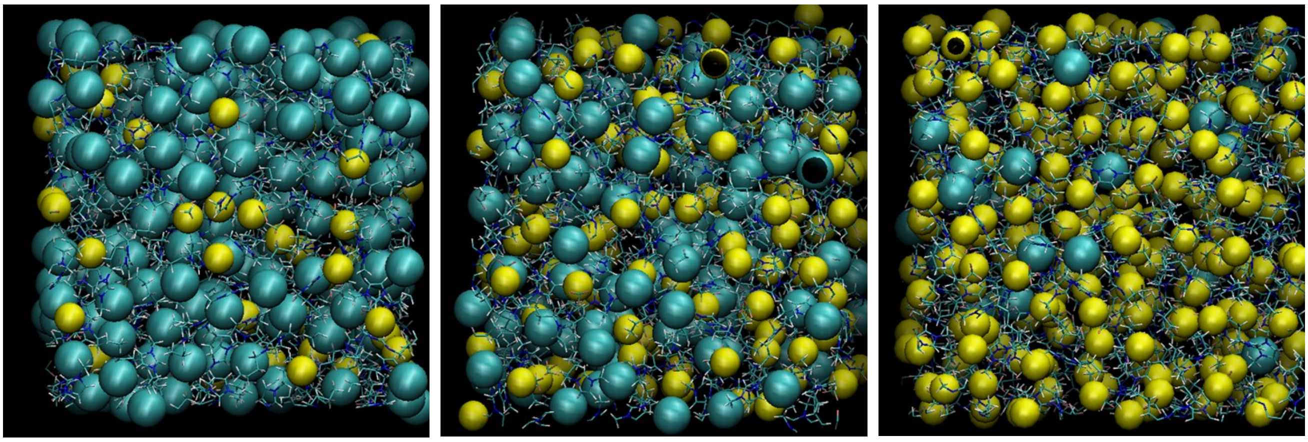

Fig. S7 Snap shot of a single trajectory frame showing the even distribution of the anions within the solution for the $[C_4C_1im]Cl_x[OTf]_{1-x}$ mixtures where x=0.2, 0.5 and 0.8. Ions are represented as stick structures, Cl ions as cyan spheres and sulfur atoms shown as yellow spheres.

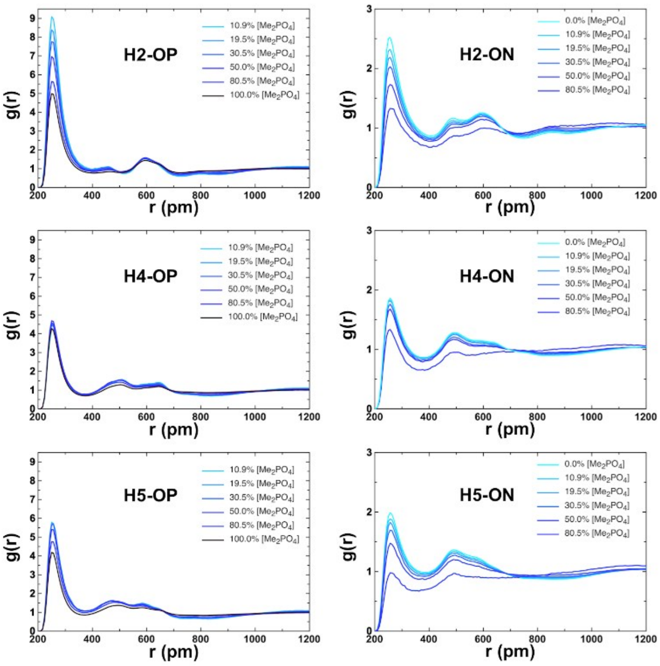

Fig. S8 Calculated RDFs for H^2,H^4 and H^5 ring protons relative to the free O's of $[Me_2PO_4]^-$ (**OP**) and O's of $[NTf_2]^-$ (**ON**) in the $[C_4C_1im][Me_2PO_4]_x[NTf_2]_{1-x}$ mixtures.

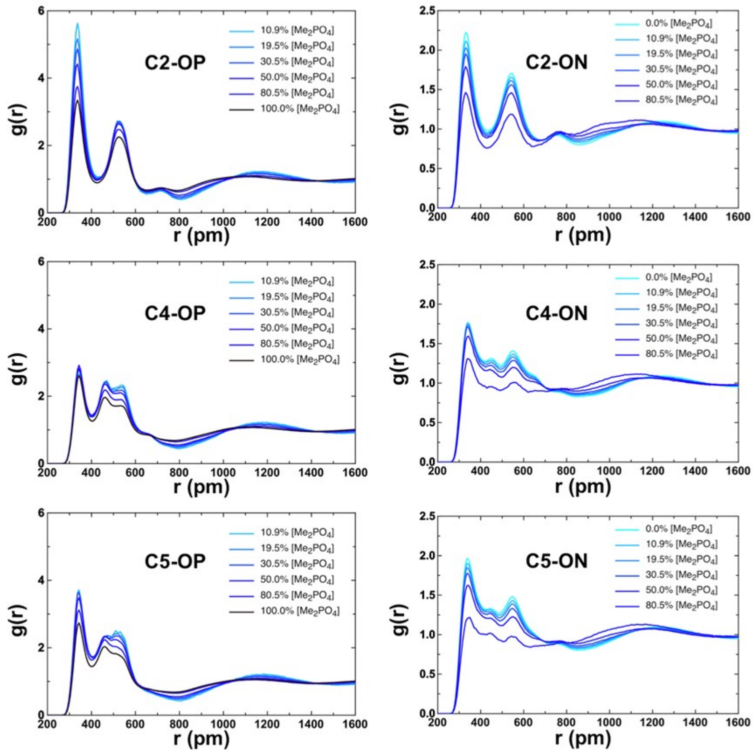

Fig. S9 Calculated RDF for C^2, C^4 and C^5 ring carbons relative to the free O's of $[Me_2PO_4]^-$ (OP) and O's of $[NTf_2]^-$ (ON) in the $[C_4C_1im][Me_2PO_4]_x[NTf_2]_{1-x}$ mixtures.

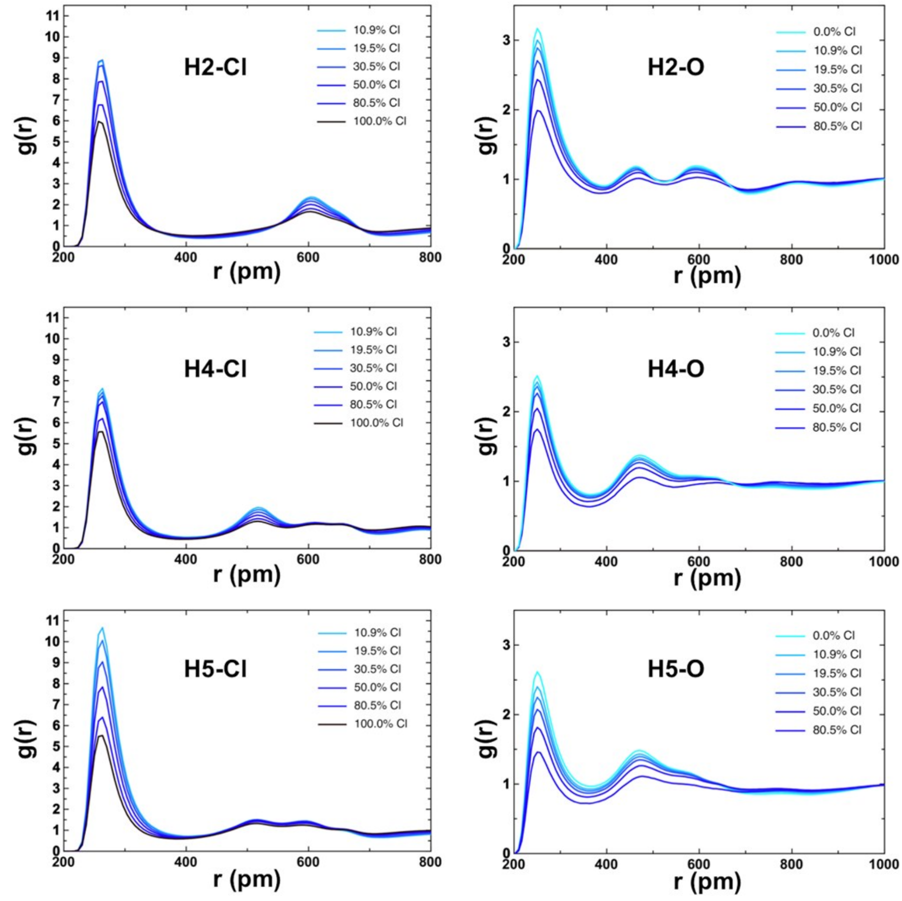

Fig. S10 Calculated RDFs for H^2, H^4 and H^5 ring protons relative to Cl^- and the O's of $[OTf]^-$ in the $[C_4C_1im]Cl_x[OTf]_{1-x}$ mixtures.

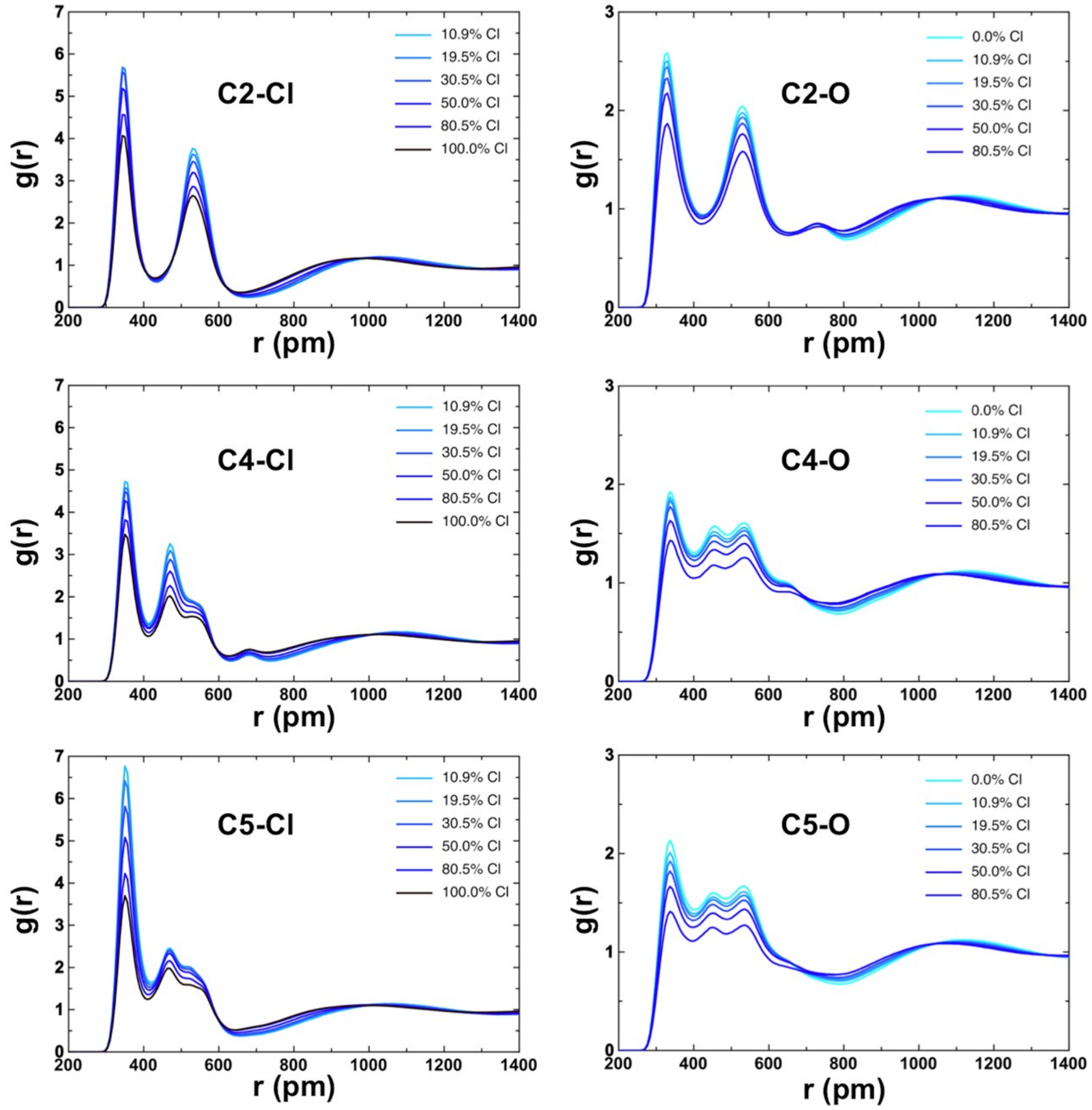

Fig. S11 Calculated RDFs for C^2, C^4, C^5 ring carbons relative to Cl^- and the O's of $[OTf]^-$ in the $[C_4C_1im]Cl_x[OTf]_{1-x}$ mixtures.

Table S5. Atom-atom distances from the QC structures.

	H^2…Cl	H^2…Cl	C^2…Cl	C^2…Cl
M_FS_SF_A	2.3208	5.7134	3.1411	4.9651
M_FS_SF_R	2.2358	5.4430	3.1821	4.7191
D_FT_TF_A	2.2578	3.1478	2.9902	3.2652
D_FT_TF_T	2.2681	3.1131	2.9787	3.2760

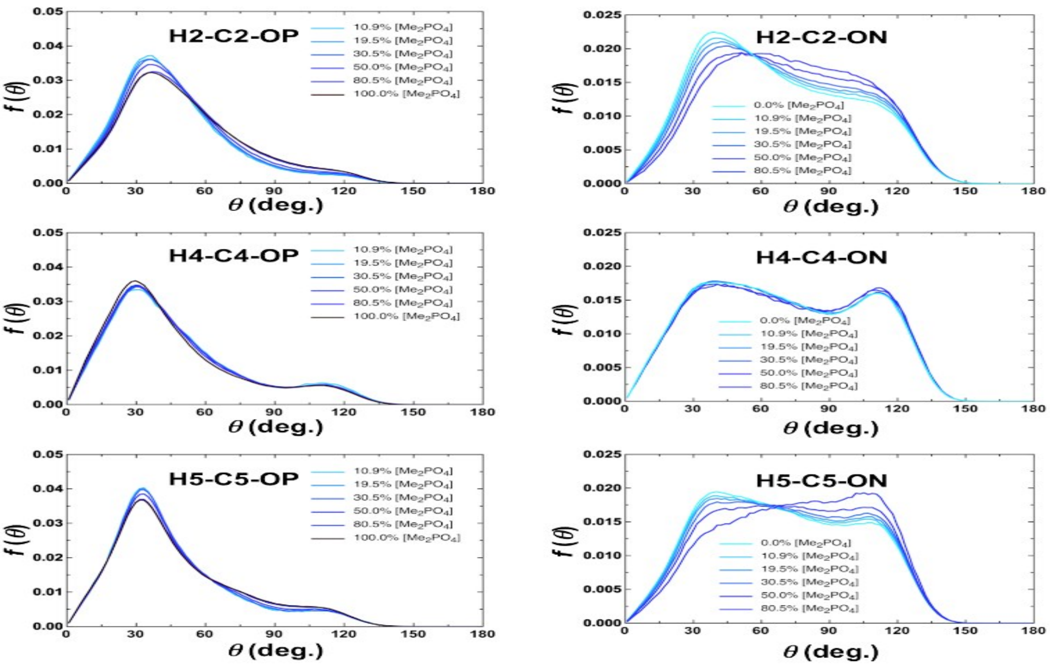

Fig. S12 Distribution of angles θ(X^-•••C^n–H^n) for atoms, within the respective cutoff distances, in the $[C_4C_1im][Me_2PO_4]_x[NTf_2]_{1-x}$ mixtures.

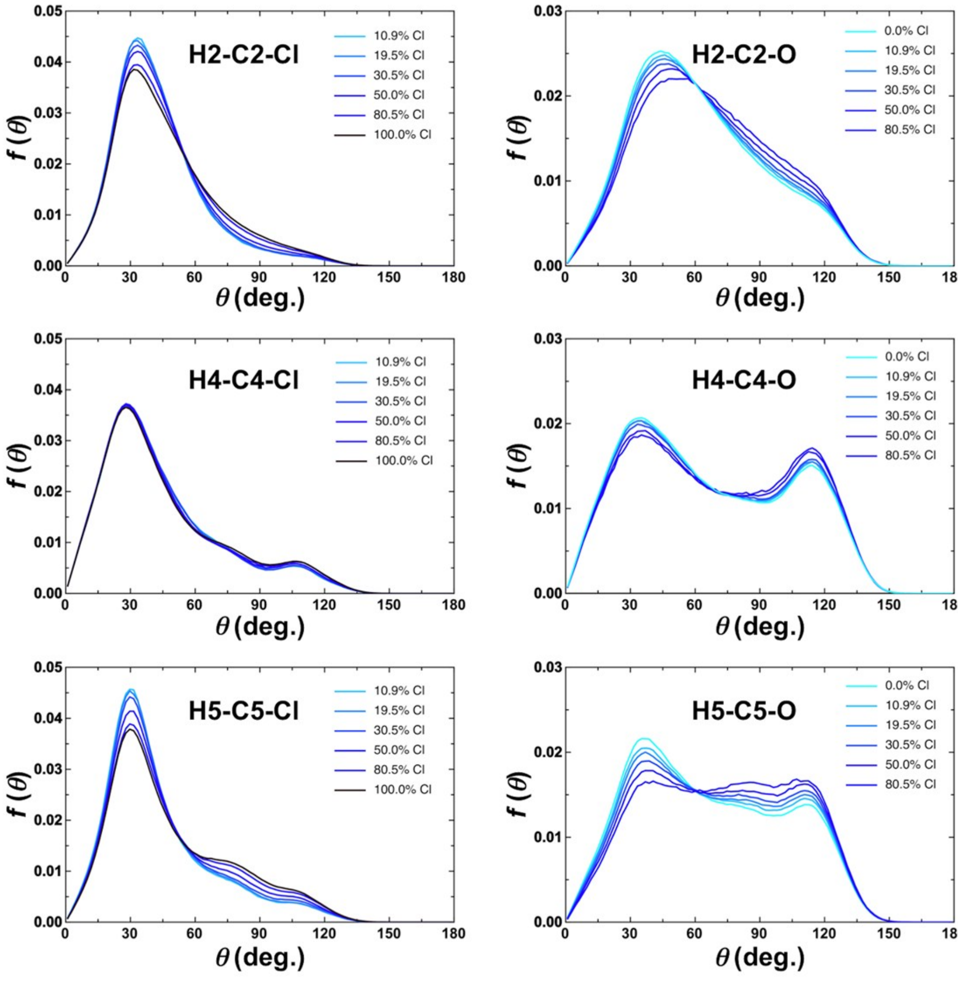

Figure S13. Distribution of angles θ(X^-•••C^n–H^n) for atoms, within the respective cutoff distances, in the $[C_4C_1im]Cl_x[OTf]_{1-x}$ mixtures.

To gain further insight into the local cation-anion structure, angular distribution functions (ADFs) have been computed for each mixture relative to the cation ring protons. First H-bonds where identified by a distance criteria, corresponding to the first minimum in the $R_{H–X}$ and $R_{C–X}$ RDFs. The normalised probability density distributions $f(\theta)$ of angles θ with values between $\theta + d\theta/2$ and $\theta - d\theta/2$ for $H^n–C^n–A^-$ (n=2,4 and 5 and A=anion) are presented, for $[Me_2PO_4]^-$ and $[NTf_2]^-$ Fig. S12 and for Cl^- and $[OTf]^-$ Fig. S13.

As the proportion of $[Me_2PO_4]^-$ increases the ADFs for H^2 and H^5 and $[Me_2PO_4]^-$ show a slight decrease in intensity at the peak maximum for angles ≈30º and an increase in the intensity for larger angles ≈60º–120º. This may be rationalised as a slight dominance of in-plane interactions with $[Me_2PO_4]^-$ at low $[Me_2PO_4]^-$ proportions, with increasing proportions leading to the anion taking up positions above and below the plane of the ring. These effects are relatively small compared to the absolute value of the probability density distribution, indicating that regardless of the proportion of $[Me_2PO_4]^-$ anions in the mixture, the preference is for in-plane rather than axial interactions with the imidazolium ring. Nonetheless, it is indicative of a similar crowding out effect to that observed in the RDF for $[Me_2PO_4]^-$ anions. Analysis of H^2 and H^5 for $[NTf_2]^-$ reveal broad distributions with two maxima, one at ≈30-50º and the other at ≈120º. As the proportion of $[Me_2PO_4]^-$ increases the first maximum decreases in intensity and the second grows. These results indicate the partial displacement of $[NTf_2]^-$ anions from in-plane H^2 or H^5 H-bonding interactions towards positions above or below the cation ring. Very little change is observed for the H^4 distributions. Similar conclusions can be drawn for the $[C_4C_1im]Cl_x[OTf]_{1-x}$ mixtures with Cl^- behaving in a similar fashion to $[Me_2PO_4]^-$ and $[OTf]^-$ like $[NTf_2]^-$.

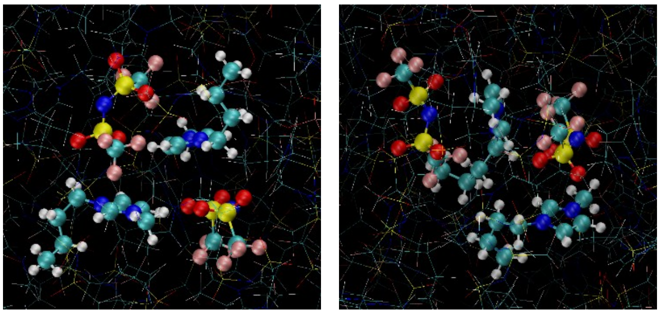

Fig. S14 Snapshots of particular structures within the $[C_4C_1im][Me_2PO_4]_{0.2}[NTf_2]_{0.8}$ mixture which has the longest (≈8-10Å) ring-ring radial distribution maximum, showing (left) an alternating IP-dimer and (right) a T-shaped IP-dimer structure.

Table S6. Computational densities (g cm^{-3}) and simulation box lengths (Å).

x	$[C_4C_1im]Cl_x[OTf]_{1-x}$		$[C_4C_1im][Me_2PO_4]_x[NTf_2]_{1-x}$	
	Density	Box Length	Density	Box Length
0	1.2877	45.8062	1.4258	50.2438
10.5	1.2718	45.3259	1.3942	49.8948
19.5	1.2450	45.0951	1.3799	49.5051
30.5	1.2288	44.5661	1.3566	49.0232
50	1.1829	43.7536	1.2705	48.6732
80	1.0935	42.5393	1.1663	47.6227
100	1.0444	41.4473	1.1003	46.7542

The normalised first-shell coordination numbers were computed for H^2 for both $[C_4C_1im]Cl_x[OTf]_{1-x}$ and $[C_4C_1im][Me_2PO_4]_x[NTf_2]_{1-x}$ mixtures and are illustrated in Figs S15 and S16. From these figures it is apparent that the more strongly H-bond accepting anion has a normalised coordination number greater than its mole fraction in the mixture, i.e. there is a local enrichment in $Cl^-/[Me_2PO_4]^-$ anions around the H^2 atom. This accords with the undiluted NMR experiments for these mixtures which found a local enrichment of these anions around H^2.

The local enrichment around H^2 determined for the $[C_4C_1im]Cl_x[OTf]_{1-x}$ and $[C_4C_1im][Me_2PO_4]_x[NTf_2]_{1-x}$ mixtures is substantially less than determined by Payal et al. for $[C_4C_1im]Cl_x[PF_6]_{1-x}$ mixtures.[29] The major rationalisation for this discrepancy lies with the different temperatures the simulations were conducted at (400 K here compared to 300 K for Payal *et al.*). At 300 K, $[C_4C_1im]Cl$ is a supercooled liquid which would greatly restrict the dynamics of the IL and increase the dependence of the coordination numbers obtained on the initial configuration. Hence, the greater thermal energy at 400 K, above the melting point of $[C_4C_1im]Cl$, will increase ion mobility,[30] reduce H-bonding lifetimes and therefore likely reduce the magnitude of preferential interactions, accounting for the difference observed.

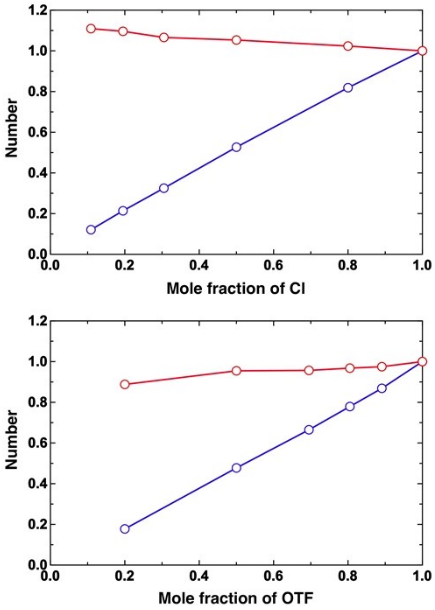

Fig. S15 Normalised first-shell coordination number of H^2 with the anion as a function of mole fraction of the anion within $[C_4C_1im]Cl_x[OTf]_{1-x}$ mixtures for (top) Cl^- and (bottom) $[OTf]^-$. Blue circles represent the normalised coordination numbers and red circles are the ratio of the normalised coordination numbers to the anion mole fraction.

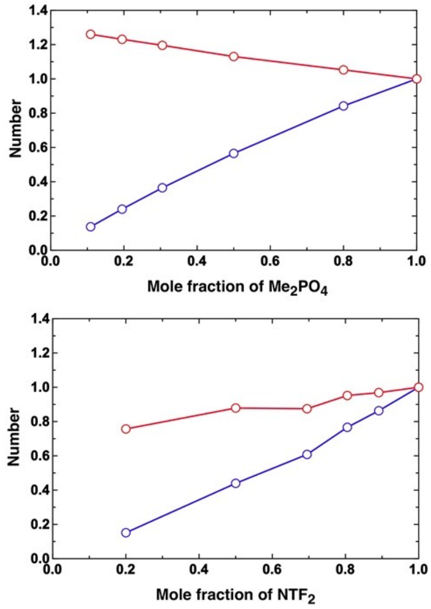

Fig. S16 Normalised first-shell coordination number of H^2 with the anion as a function of mole fraction of the anion within $[C_4C_1im][Me_2PO_4]_x[NTf_2]_{1-x}$ mixtures for (top) $[Me_2PO_4]^-$ and (bottom) $[NTf_2]^-$. Blue circles represent the normalised coordination numbers and red circles are the ratio of the normalised coordination numbers to the anion mole fraction.

Section C: Dichloromethane-d_2 Experiments

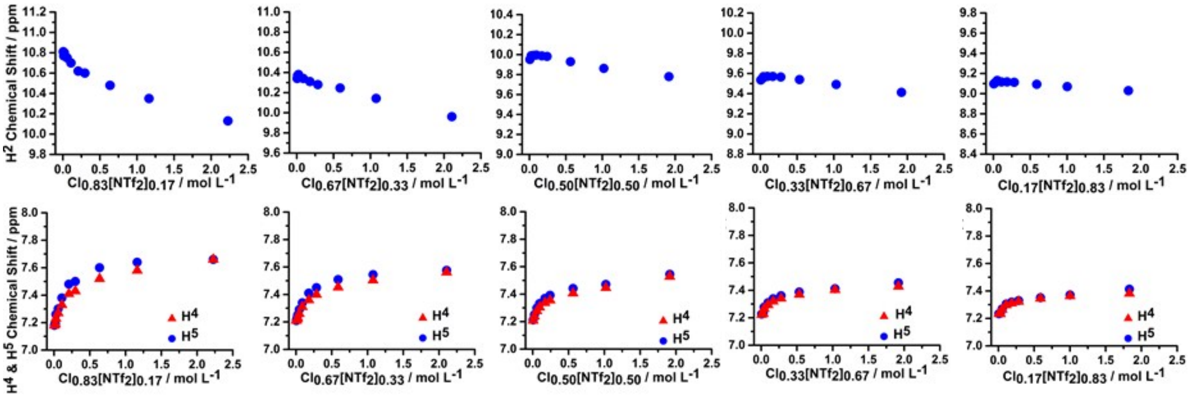

Fig. S17 ^{1}H NMR chemical shifts of the H^2, H^4 and H^5 signals of [C$_4$C$_1$im]Cl$_x$[NTf$_2$]$_{1-x}$ mixtures at various concentrations in CD$_2$Cl$_2$.

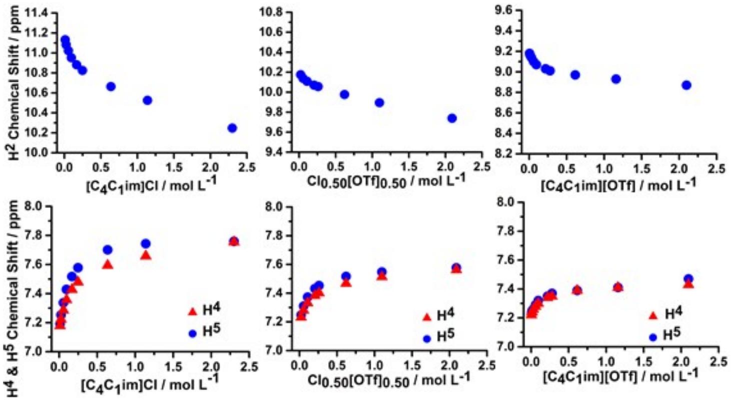

Fig. S18 ^{1}H NMR chemical shifts of the H^2, H^4 and H^5 signals of [C$_4$C$_1$im]Cl, [C$_4$C$_1$im]Cl$_{0.50}$[OTf]$_{0.50}$ and [C$_4$C$_1$im][OTf] at various concentrations in CD$_2$Cl$_2$.

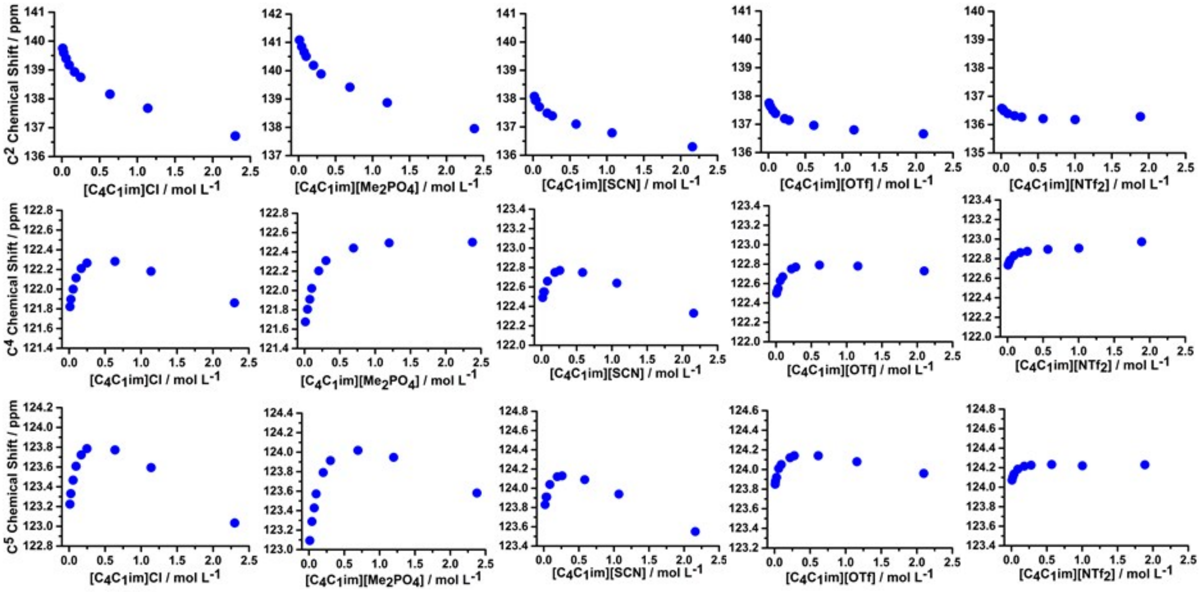

Fig. S19 ^{13}C chemical shifts of the C^2, C^4 and C^5 signals from the simple ILs at various concentrations in CD$_2$Cl$_2$.

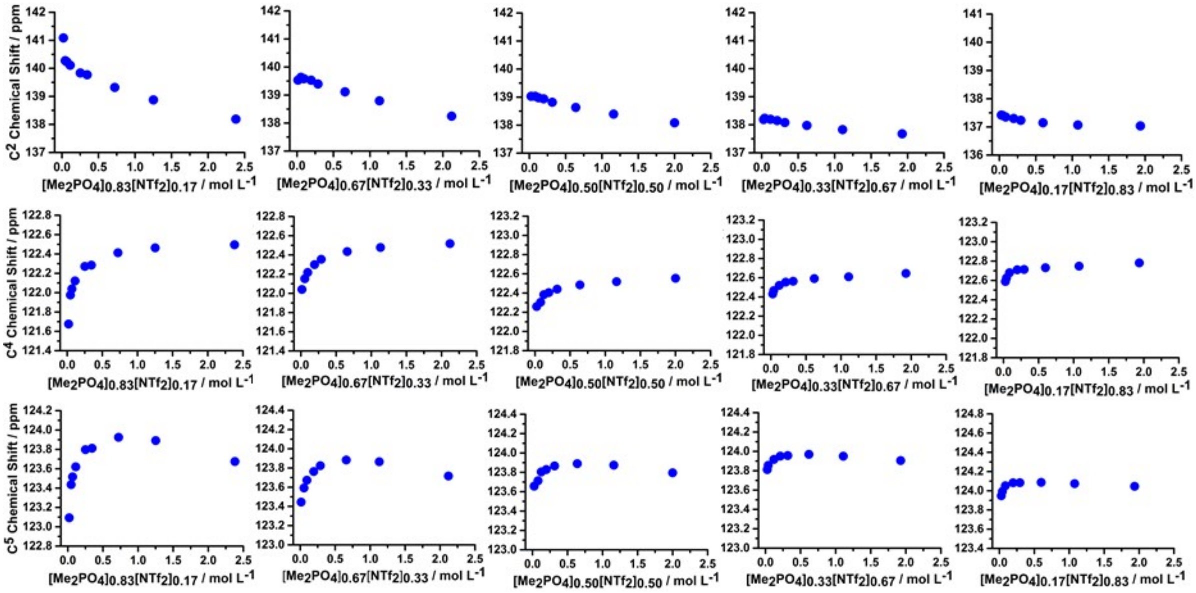

Fig. S20 ^{13}C chemical shift of the C^2, C^4 and C^5 signals from $[C_4C_1im][Me_2PO_4]_x[NTf_2]_{1-x}$ mixtures at various concentrations in CD_2Cl_2.

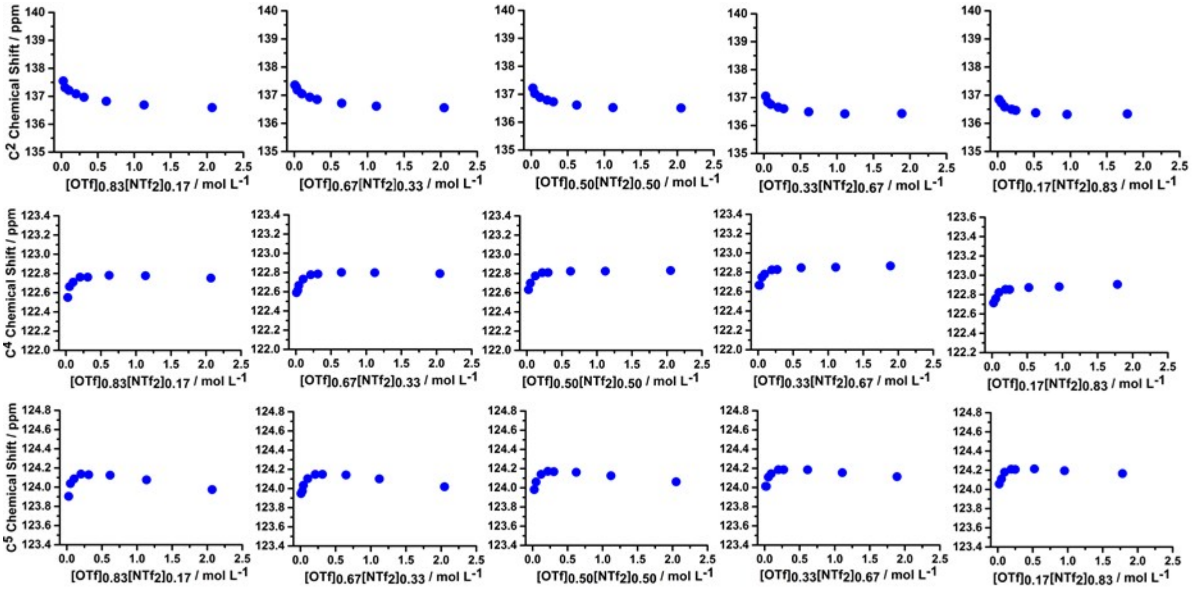

Fig. S21 ^{13}C chemical shift of the C^2, C^4 and C^5 signals from $[C_4C_1im][OTf]_x[NTf_2]_{1-x}$ mixtures at various concentrations in CD_2Cl_2.

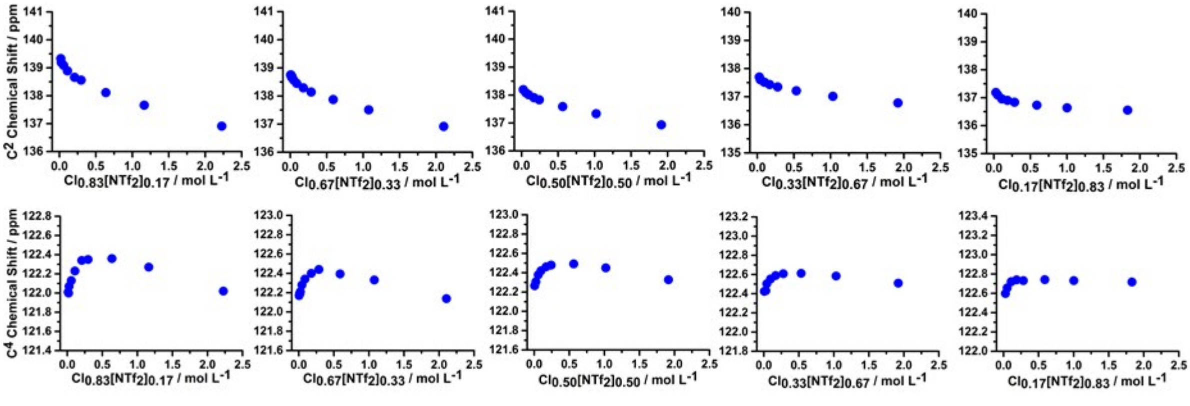

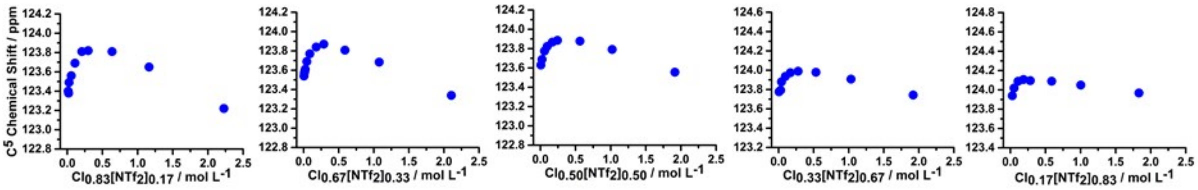

Fig. S22 ^{13}C chemical shift of the C^2, C^4 and C^5 signals from $[C_4C_1im]Cl_x[NTf_2]_{1-x}$ mixtures at various concentrations in CD_2Cl_2.

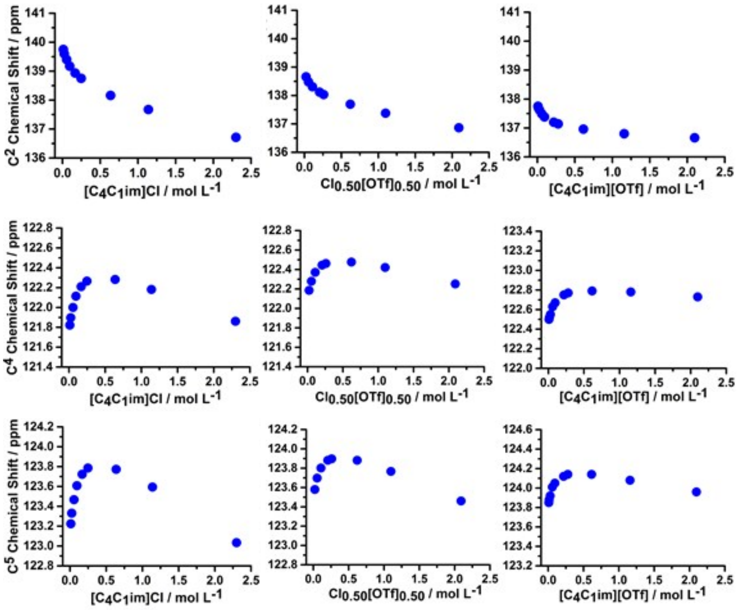

Fig. S23 ^{13}C chemical shift of the C^2, C^4 and C^5 signals from $[C_4C_1im]Cl$, $[C_4C_1im]Cl_{0.50}[OTf]_{0.50}$ and $[C_4C_1im][OTf]$ at various concentrations in CD_2Cl_2.

Table S7. NMR chemical shifts of dichloromethane-d_2 experiments for $[C_4C_1im]Cl$.

Concentration (mol L^{-1})	H^2	H^4	H^5	C^2	C^4	C^5
0.011	11.132	7.179	7.192	139.750	121.822	123.224
0.024	11.083	7.224	7.253	139.601	121.897	123.331
0.056	11.022	7.286	7.337	139.401	122.000	123.467
0.096	10.952	7.357	7.429	139.174	122.114	123.608
0.168	10.881	7.428	7.517	138.936	122.210	123.723
0.247	10.825	7.479	7.578	138.752	122.266	123.786
0.637	10.663	7.594	7.701	138.164	122.282	123.773
1.139	10.526	7.658	7.743	137.674	122.181	123.594
2.300	10.247	7.755	7.759	136.711	121.861	123.034

Table S8. NMR chemical shifts of dichloromethane-d_2 experiments for $[C_4C_1im][Me_2PO_4]$.

Concentration (mol L^{-1})	**H^2**	**H^4**	**H^5**	**C^2**	**C^4**	**C^5**
0.011	10.886	7.140	7.140	141.085	121.676	123.093
0.042	10.825	7.199	7.234	140.849	121.806	123.288
0.075	10.770	7.245	7.296	140.658	121.909	123.428
0.101	10.746	7.299	7.369	140.509	122.023	123.572
0.202	10.669	7.393	7.488	140.190	122.204	123.791
0.304	10.587	7.459	7.567	139.885	122.310	123.913
0.693	10.465	7.564	7.674	139.418	122.440	124.018
1.198	10.318	7.665	7.738	138.870	122.493	123.947
2.378	10.056	7.773	7.837	137.954	122.501	123.581

Table S9. NMR chemical shifts of dichloromethane-d_2 experiments for $[C_4C_1im][SCN]$.

Concentration (mol L^{-1})	**H^2**	**H^4**	**H^5**	**C^2**	**C^4**	**C^5**
0.006	9.52	7.26	7.26	NA[a]	NA[a]	NA[a]
0.012	9.55	7.23	7.23	NA[a]	NA[a]	NA[a]
0.018	9.51	7.26	7.26	138.08	122.49	123.83
0.032	9.48	7.29	7.3	137.94	122.55	123.91
0.042	9.47	7.29	7.3	137.94	122.55	123.91
0.086	9.42	7.35	7.37	137.71	122.66	124.04
0.191	9.37	7.4	7.43	137.49	122.75	124.12
0.261	9.35	7.42	7.45	137.39	122.77	124.13
0.584	9.29	7.47	7.5	137.1	122.75	124.09
1.070	9.23	7.5	7.51	136.79	122.64	123.94
2.160	9.11	7.51	7.53	136.3	122.33	123.55

[a] No ^{13}C signal was detected due to low concentration

Table S10. NMR chemical shifts of dichloromethane-d_2 experiments for $[C_4C_1im][OTf]$.

Concentration (mol L^{-1})	**H^2**	**H^4**	**H^5**	**C^2**	**C^4**	**C^5**
0.005	9.18	7.22	7.23	NA[a]	NA[a]	NA[a]
0.009	9.17	7.24	7.24	137.75	122.5	123.85
0.014	9.16	7.24	7.25	137.69	122.52	123.88
0.029	9.14	7.26	7.26	137.62	122.55	123.92
0.059	9.1	7.28	7.29	137.49	122.63	124.01
0.095	9.07	7.3	7.32	137.38	122.67	124.05
0.219	9.03	7.34	7.35	137.2	122.75	124.12
0.279	9.01	7.35	7.37	137.14	122.77	124.14
0.615	8.97	7.39	7.39	136.96	122.79	124.14
1.158	8.93	7.41	7.41	136.8	122.78	124.08
2.098	8.87	7.43	7.47	136.66	122.73	123.96

[a] No ^{13}C signal was detected due to low concentration

Table S11. NMR chemical shifts of dichloromethane-*d*$_2$ experiments for [C_4C_1im][NTf_2].

Concentration (mol L^{-1})	**H^2**	**H^4**	**H^5**	**C^2**	**C^4**	**C^5**
0.009	8.682	7.250	7.250	136.575	122.735	124.073
0.022	8.668	7.258	7.262	136.552	122.760	124.106
0.037	8.656	7.266	7.270	136.491	122.785	124.135
0.090	8.631	7.282	7.285	136.390	122.831	124.185
0.182	8.612	7.295	7.301	136.311	122.862	124.215
0.278	8.601	7.302	7.309	136.265	122.875	124.226
0.568	8.583	7.313	7.323	136.209	122.895	124.233
1.002	8.569	7.325	7.345	136.177	122.907	124.220
1.886	8.557	7.343	7.386	136.284	122.972	124.230

Table S12. NMR chemical shifts of dichloromethane-*d*$_2$ experiments for [C_4C_1im][Me_2PO_4]$_{0.83}$[NTf_2]$_{0.17}$.

Concentration (mol L^{-1})	**H^2**	**H^4**	**H^5**	**C^2**	**C^4**	**C^5**
0.020	10.146	7.170	7.174	141.085	121.676	123.093
0.046	10.557	7.219	7.249	140.276	121.976	123.436
0.068	10.570	7.250	7.291	140.232	122.039	123.517
0.112	10.556	7.293	7.347	140.111	122.122	123.620
0.251	10.496	7.373	7.446	139.835	122.272	123.798
0.344	10.488	7.387	7.463	139.772	122.285	123.812
0.722	10.373	7.487	7.569	139.322	122.413	123.925
1.251	10.253	7.571	7.629	138.877	122.464	123.891
2.380	10.051	7.680	7.710	138.190	122.496	123.675

Table S13. NMR chemical shifts of dichloromethane-*d*$_2$ experiments for [C_4C_1im][Me_2PO_4]$_{0.67}$[NTf_2]$_{0.33}$.

Concentration (mol L^{-1})	**H^2**	**H^4**	**H^5**	**C^2**	**C^4**	**C^5**
0.013	10.084	7.177	7.181	139.532	122.041	123.445
0.025	10.199	7.199	7.211	-	-	-
0.054	10.253	7.241	7.267	139.633	122.152	123.592
0.096	10.272	7.275	7.311	139.583	122.218	123.673
0.193	10.309	7.323	7.369	139.529	122.299	123.763
0.288	10.284	7.356	7.408	139.396	122.355	123.824
0.658	10.228	7.428	7.482	139.114	122.435	123.883
1.130	10.144	7.493	7.532	138.794	122.478	123.865
2.120	9.981	7.588	7.616	138.247	122.518	123.717

Table S14. NMR chemical shifts of dichloromethane-d_2 experiments for $[C_4C_1im][Me_2PO_4]_{0.50}[NTf_2]_{0.50}$.

Concentration (mol L^{-1})	H^2	H^4	H^5	C^2	C^4	C^5
0.009	9.798	7.188	7.192	NA[a]	NA[a]	NA[a]
0.024	9.926	7.226	7.237	139.030	122.259	123.657
0.079	9.960	7.249	7.267	139.029	122.304	123.714
0.125	9.988	7.291	7.318	138.977	122.383	123.805
0.197	9.985	7.303	7.333	138.938	122.405	123.829
0.315	9.981	7.336	7.369	138.817	122.441	123.866
0.639	9.948	7.383	7.415	138.630	122.485	123.890
1.161	9.891	7.436	7.455	138.394	122.519	123.874
2.000	9.795	7.498	7.520	138.083	122.554	123.796

[a] No ^{13}C signal was detected due to low concentration

Table S15. NMR chemical shifts of dichloromethane-d_2 experiments for $[C_4C_1im][Me_2PO_4]_{0.33}[NTf_2]_{0.67}$.

Concentration (mol L^{-1})	H^2	H^4	H^5	C^2	C^4	C^5
0.005	9.444	7.210	7.214	NA[a]	NA[a]	NA[a]
0.026	9.495	7.236	7.239	138.185	122.431	123.812
0.040	9.546	7.255	7.265	138.229	122.466	123.855
0.120	9.573	7.284	7.299	138.194	122.521	123.917
0.212	9.581	7.304	7.321	138.149	122.554	123.951
0.318	9.579	7.319	7.337	138.077	122.563	123.957
0.619	9.570	7.350	7.365	137.977	122.591	123.969
1.109	9.539	7.390	7.394	137.826	122.610	123.950
1.926	9.489	7.429	7.454	137.676	122.645	123.905

[a] No ^{13}C signal was detected due to low concentration

Table S16. NMR chemical shifts of dichloromethane-d_2 experiments for $[C_4C_1im][Me_2PO_4]_{0.17}[NTf_2]_{0.83}$.

Concentration (mol L^{-1})	H^2	H^4	H^5	C^2	C^4	C^5
0.007	9.084	7.234	7.238	NA[a]	NA[a]	NA[a]
0.027	9.095	7.240	7.244	137.420	122.589	123.948
0.043	9.113	7.258	7.262	137.408	122.626	123.994
0.086	9.124	7.283	7.287	137.352	122.680	124.053
0.196	9.123	7.301	7.303	137.298	122.710	124.083
0.294	9.119	7.310	7.313	137.234	122.713	124.084
0.598	9.105	7.331	7.335	137.148	122.731	124.087
1.077	9.087	7.353	7.362	137.068	122.748	124.074
1.936	9.060	7.380	7.414	137.036	122.781	124.046

[a] No ^{13}C signal was detected due to low concentration

Table S17. NMR chemical shifts of dichloromethane-d_2 experiments for $[C_4C_1im][OTf]_{0.83}[NTf_2]_{0.17}$.

Concentration (mol L^{-1})	H^2	H^4	H^5	C^2	C^4	C^5
0.010	9.098	7.227	7.231	NA[a]	NA[a]	NA[a]
0.026	9.085	7.241	7.245	137.549	122.551	123.905
0.051	9.026	7.283	7.293	137.311	122.664	124.038
0.103	9.003	7.303	7.314	137.214	122.710	124.087
0.202	8.972	7.328	7.340	137.089	122.762	124.137
0.310	8.951	7.346	7.357	136.968	122.762	124.130
0.617	8.917	7.378	7.378	136.824	122.781	124.125
1.136	8.881	7.399	7.408	136.691	122.777	124.077
2.070	8.832	7.418	7.455	136.596	122.752	123.975

[a] No ^{13}C signal was detected due to low concentration

Table S18. NMR chemical shifts of dichloromethane-d_2 experiments for $[C_4C_1im][OTf]_{0.67}[NTf_2]_{0.33}$.

Concentration (mol L^{-1})	H^2	H^4	H^5	C^2	C^4	C^5
0.009	9.005	7.241	7.245	137.363	122.591	123.948
0.027	8.990	7.255	7.259	137.289	122.615	123.973
0.041	8.962	7.275	7.281	137.185	122.666	124.033
0.103	8.931	7.300	7.309	137.050	122.732	124.103
0.211	8.904	7.325	7.334	136.930	122.778	124.147
0.312	8.888	7.337	7.345	136.849	122.785	124.148
0.648	8.857	7.364	7.368	136.714	122.802	124.141
1.121	8.829	7.383	7.394	136.611	122.799	124.100
2.047	8.788	7.402	7.440	136.554	122.789	124.018

Table S19. NMR chemical shifts of dichloromethane-d_2 experiments for $[C_4C_1im][OTf]_{0.50}[NTf_2]_{0.50}$.

Concentration (mol L^{-1})	H^2	H^4	H^5	C^2	C^4	C^5
0.008	8.908	7.236	7.240	NA[a]	NA[a]	NA[a]
0.023	8.925	7.246	7.250	137.220	122.632	123.982
0.049	8.892	7.273	7.277	137.026	122.700	124.061
0.121	8.858	7.302	7.305	136.890	122.776	124.141
0.218	8.835	7.320	7.324	136.791	122.809	124.172
0.303	8.825	7.329	7.332	136.730	122.810	124.169
0.624	8.798	7.351	7.355	136.613	122.824	124.162
1.119	8.773	7.368	7.382	136.522	122.825	124.126
2.051	8.738	7.388	7.428	136.508	122.831	124.063

[a] No ^{13}C signal was detected due to low concentration

Table S20. NMR chemical shifts of dichloromethane-d_2 experiments for $[C_4C_1im][OTf]_{0.33}[NTf_2]_{0.67}$.

Concentration (mol L^{-1})	H^2	H^4	H^5	C^2	C^4	C^5
0.014	8.851	7.243	7.247	NA[a]	122.667	124.013
0.024	8.850	7.244	7.248	137.052	122.667	124.012
0.054	8.809	7.276	7.280	136.838	122.750	124.108
0.093	8.793	7.290	7.294	136.758	122.782	124.143
0.196	8.768	7.310	7.314	136.657	122.826	124.186
0.272	8.759	7.316	7.320	136.603	122.829	124.186
0.614	8.731	7.338	7.344	136.489	122.848	124.185
1.108	8.710	7.354	7.371	136.419	122.853	124.155
1.888	8.687	7.370	7.408	136.428	122.867	124.113

[a] No ^{13}C signal was detected due to low concentration

Table S21. NMR chemical shifts of dichloromethane-d_2 experiments for $[C_4C_1im][OTf]_{0.17}[NTf_2]_{0.83}$.

Concentration (mol L^{-1})	H^2	H^4	H^5	C^2	C^4	C^5
0.008	8.769	7.243	7.243	NA[a]	NA[a]	NA[a]
0.021	8.767	7.248	7.252	136.846	122.714	124.057
0.052	8.745	7.264	7.268	136.726	122.758	124.109
0.098	8.711	7.288	7.292	136.584	122.822	124.180
0.192	8.692	7.303	7.307	136.500	122.854	124.211
0.250	8.685	7.307	7.311	136.461	122.853	124.208
0.524	8.664	7.323	7.331	136.375	122.873	124.214
0.954	8.646	7.335	7.352	136.317	122.881	124.195
1.783	8.627	7.354	7.391	136.336	122.906	124.166

[a] No ^{13}C signal was detected due to low concentration

Table S22. NMR chemical shifts of dichloromethane-d_2 experiments for $[C_4C_1im]Cl_{0.83}[NTf_2]_{0.17}$.

Concentration (mol L^{-1})	H^2	H^4	H^5	C^2	C^4	C^5
0.006	10.81	7.18	7.18	NA[a]	NA[a]	NA[a]
0.013	10.77	7.19	7.19	NA[a]	122.01	123.4
0.019	10.8	7.19	7.19	139.33	122	123.38
0.026	10.77	7.23	7.26	139.19	122.07	123.49
0.057	10.75	7.27	7.3	139.09	122.13	123.56
0.110	10.7	7.33	7.38	138.89	122.23	123.69
0.208	10.62	7.41	7.48	138.66	122.34	123.81
0.298	10.6	7.43	7.5	138.56	122.35	123.82
0.637	10.48	7.52	7.6	138.11	122.36	123.81
1.163	10.35	7.58	7.64	137.66	122.27	123.65
2.227	10.13	7.66	7.66	136.91	122.02	123.22

[a] No ^{13}C signal was detected due to low concentration

Table S23. NMR chemical shifts of dichloromethane-d_2 experiments for $[C_4C_1im]Cl_{0.67}[NTf_2]_{0.33}$.

Concentration (mol L^{-1})	H^2	H^4	H^5	C^2	C^4	C^5
0.005	10.34	7.21	7.21	138.75	122.17	123.54
0.011	10.37	7.22	7.22	138.75	122.19	123.57
0.017	10.35	7.22	7.23	138.67	122.19	123.59
0.023	10.38	7.23	7.25	138.7	122.21	123.61
0.046	10.35	7.26	7.29	138.57	122.28	123.69
0.088	10.34	7.31	7.34	138.45	122.34	123.77
0.179	10.31	7.36	7.41	138.29	122.4	123.84
0.287	10.28	7.4	7.45	138.14	122.44	123.87
0.589	10.246	7.453	7.509	137.875	122.394	123.808
1.077	10.143	7.504	7.545	137.507	122.331	123.684
2.106	9.961	7.562	7.576	136.915	122.138	123.339

Table S24. NMR chemical shifts of dichloromethane-d_2 experiments for $[C_4C_1im]Cl_{0.50}[NTf_2]_{0.50}$.

Concentration (mol L^{-1})	H^2	H^4	H^5	C^2	C^4	C^5
0.006	9.951	7.208	7.212	NA[a]	122.265	123.63
0.023	9.989	7.239	7.25	138.192	122.306	123.688
0.058	9.992	7.278	7.299	138.086	122.378	123.775
0.096	9.995	7.305	7.332	138.011	122.42	123.823
0.170	9.987	7.337	7.369	137.906	122.461	123.867
0.242	9.981	7.356	7.392	137.829	122.479	123.886
0.563	9.929	7.407	7.442	137.586	122.491	123.878
1.021	9.862	7.447	7.471	137.33	122.45	123.792
1.914	9.78	7.529	7.545	136.934	122.327	123.556

[a] No ^{13}C signal was detected due to low concentration

Table S25. NMR chemical shifts of dichloromethane-d_2 experiments for $[C_4C_1im]Cl_{0.33}[NTf_2]_{0.67}$.

Concentration (mol L^{-1})	H^2	H^4	H^5	C^2	C^4	C^5
0.007	9.536	7.223	7.227	NA[a]	122.424	123.777
0.029	9.551	7.23	7.234	137.699	122.431	123.793
0.042	9.569	7.267	7.277	137.604	122.503	123.88
0.096	9.571	7.294	7.31	137.517	122.553	123.936
0.169	9.571	7.32	7.339	137.431	122.589	123.974
0.278	9.565	7.341	7.361	137.346	122.608	123.99
0.533	9.54	7.37	7.388	137.209	122.612	123.979
1.032	9.492	7.404	7.412	137.014	122.584	123.908
1.920	9.413	7.429	7.455	136.778	122.51	123.743

[a] No ^{13}C signal was detected due to low concentration

Table S26. NMR chemical shifts of dichloromethane-d_2 experiments for $[C_4C_1im]Cl_{0.17}[NTf_2]_{0.67}$.

Concentration (mol L^{-1})	H^2	H^4	H^5	C^2	C^4	C^5
0.007	9.097	7.234	7.234	NA[a]	NA[a]	NA[a]
0.028	9.111	7.233	7.237	137.186	122.598	123.939
0.052	9.131	7.265	7.269	137.098	122.656	124.019
0.110	9.116	7.298	7.305	136.957	122.72	124.089
0.187	9.117	7.311	7.319	136.906	122.74	124.107
0.284	9.113	7.323	7.33	136.839	122.732	124.096
0.589	9.093	7.346	7.351	136.733	122.742	124.09
1.002	9.07	7.364	7.371	136.638	122.732	124.05
1.832	9.03	7.382	7.413	136.555	122.717	123.968

[a] No ^{13}C signal was detected due to low concentration

Table S27. NMR chemical shifts of dichloromethane-d_2 experiments for $[C_4C_1im]Cl_{0.50}[OTf]_{0.50}$.

Concentration (mol L^{-1})	H^2	H^4	H^5	C^2	C^4	C^5
0.022	10.175	7.232	7.248	138.661	122.186	123.58
0.054	10.138	7.281	7.31	138.482	122.279	123.698
0.108	10.11	7.332	7.373	138.309	122.371	123.802
0.204	10.07	7.383	7.432	138.12	122.445	123.881
0.260	10.056	7.402	7.453	138.035	122.462	123.897
0.621	9.977	7.468	7.517	137.694	122.477	123.881
1.098	9.895	7.514	7.548	137.377	122.421	123.767
2.091	9.739	7.563	7.577	136.863	122.252	123.461

[a] No ^{13}C signal was detected due to low concentration

Section D: Undiluted Ionic Liquid NMR

^{1}H NMR Experiments

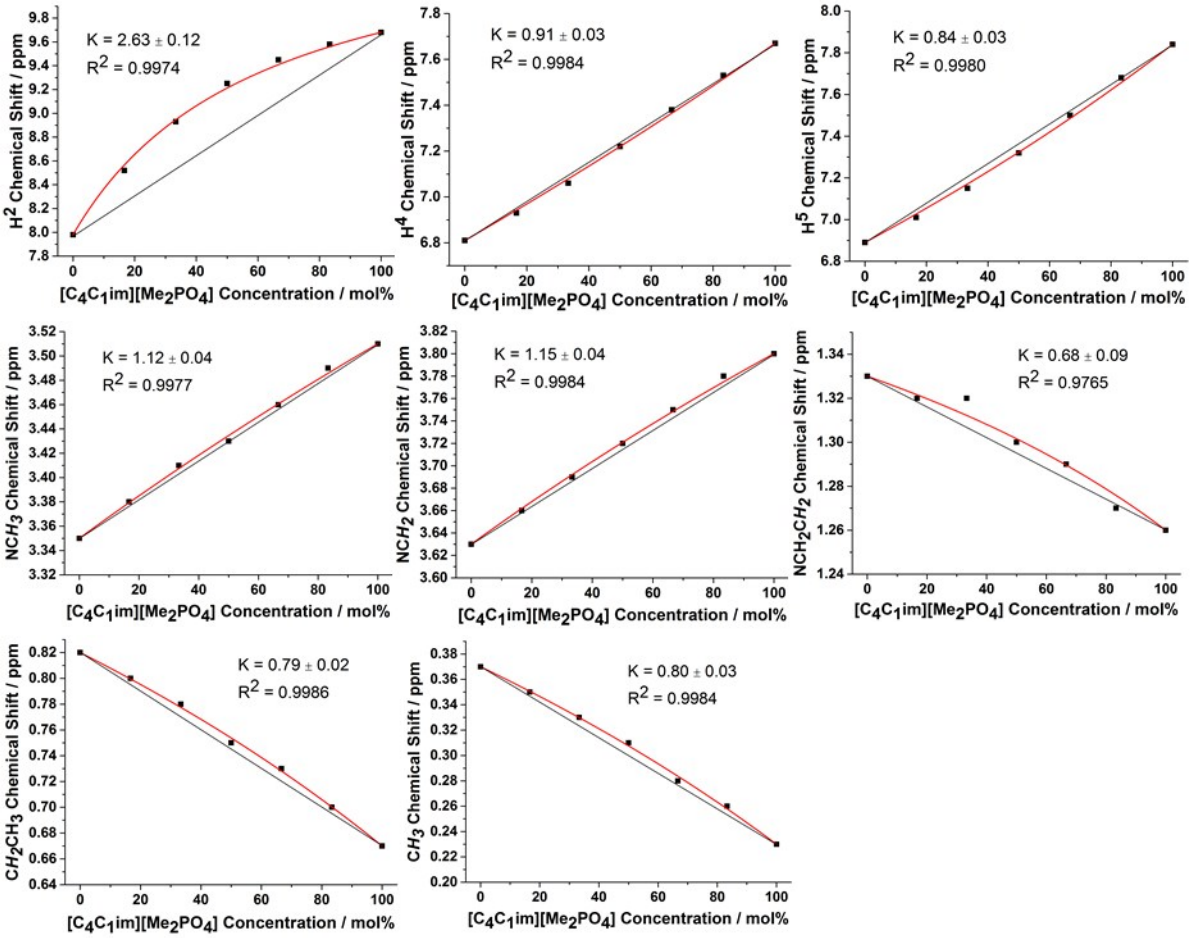

Fig. S24 ^{1}H NMR chemical shifts for different imidazolium cation shifts of $[C_4C_1im][Me_2PO_4]_x[NTf_2]_{1-x}$ mixtures referenced to an internal capillary of DMSO-d_6. Red lines represent the fitted model with given fitting parameters, black lines are drawn between both simple ILs as a guide for the eye.

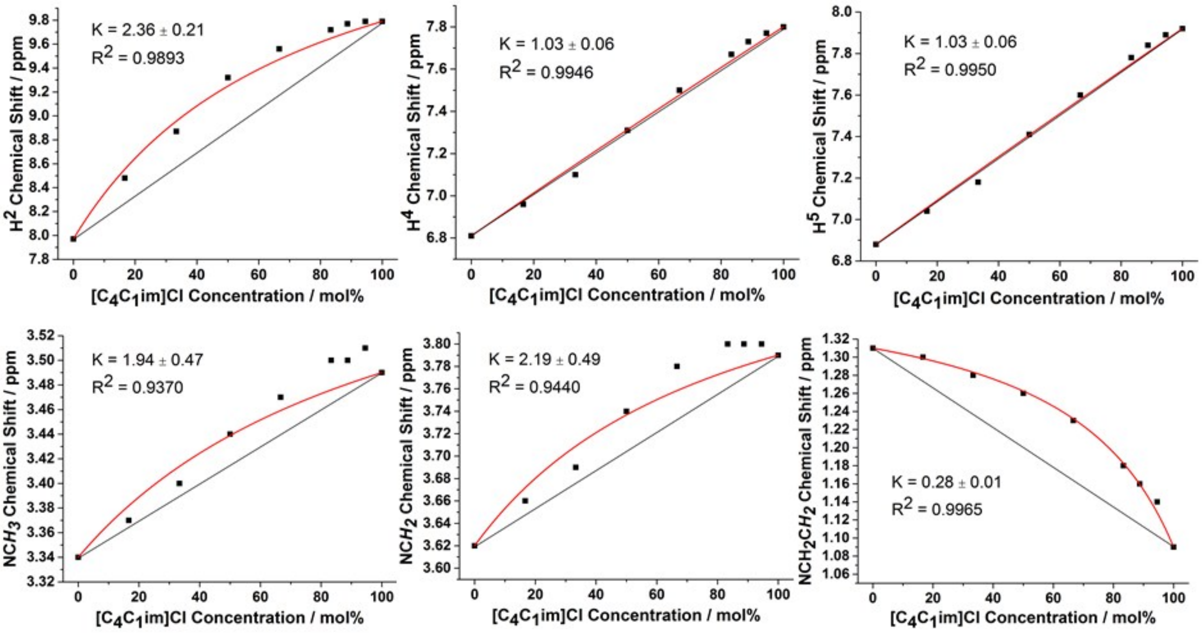

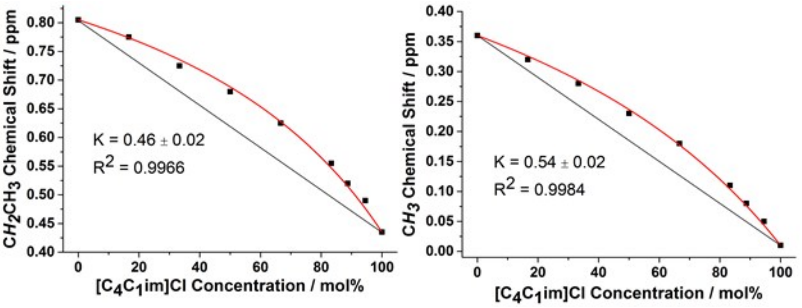

Fig. S25 ^{1}H NMR chemical shifts for different imidazolium cation shifts of $[C_4C_1im]Cl_x[NTf_2]_{1-x}$ mixtures referenced to an internal capillary of DMSO-d_6. Red lines represent the fitted model with given fitting parameters, black lines are drawn between both simple ILs as a guide for the eye.

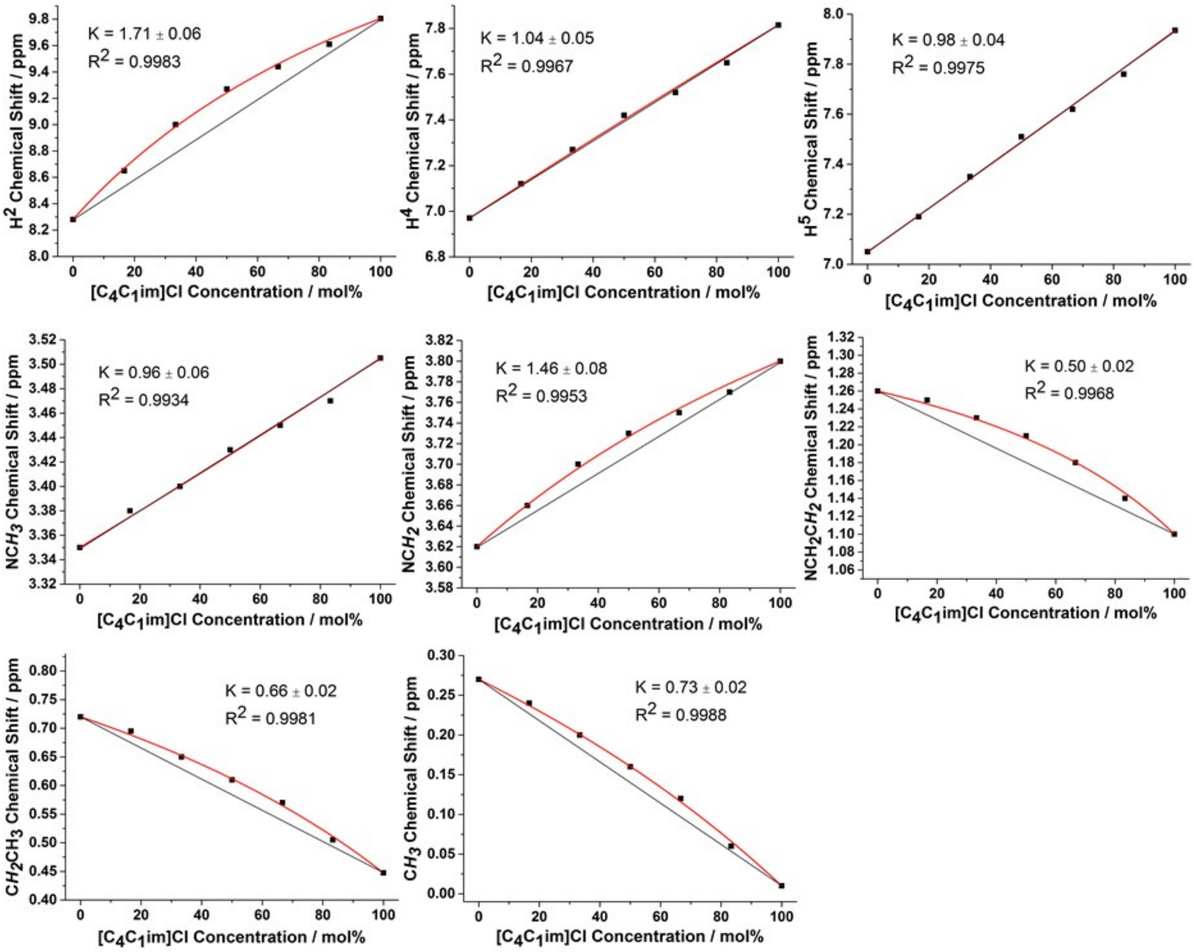

Fig. S26 ^{1}H NMR chemical shifts for different imidazolium cation shifts of $[C_4C_1im]Cl_x[OTf]_{1-x}$ mixtures referenced to an internal capillary of DMSO-d_6. Red lines represent the fitted model with given fitting parameters, black lines are drawn between both simple ILs as a guide for the eye.

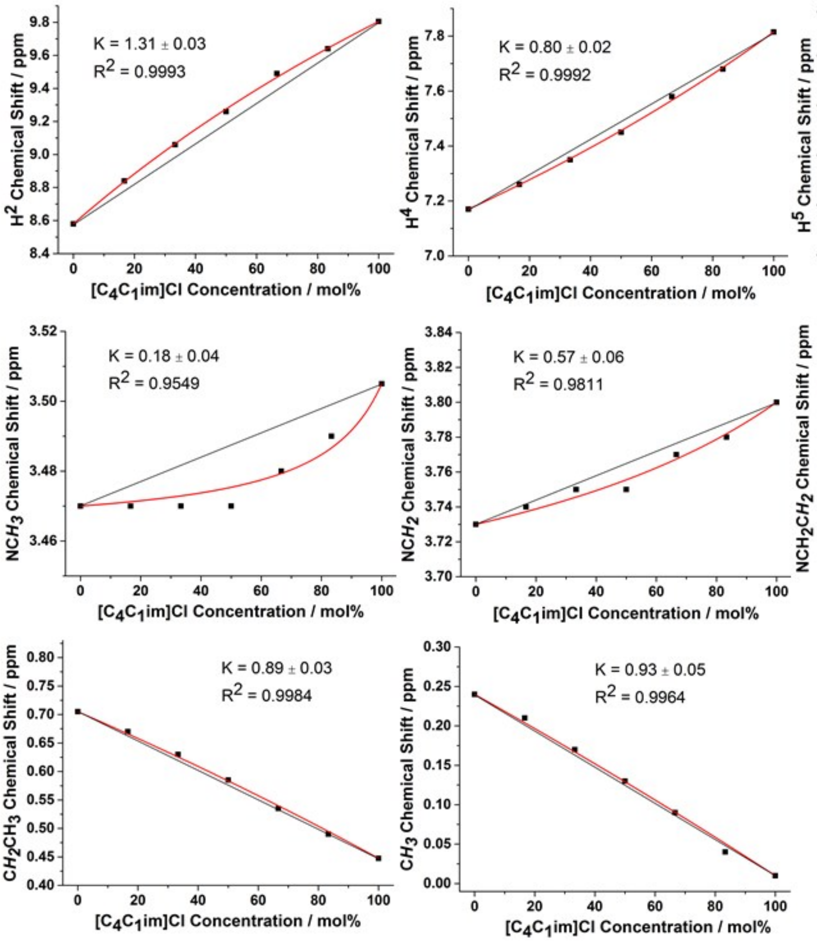

Fig. S27 ^{1}H NMR chemical shifts for different imidazolium cation shifts of $[C_4C_1im]Cl_x[SCN]_{1-x}$ mixtures referenced to an internal capillary of DMSO-d_6. Red lines represent the fitted model with given fitting parameters, black lines are drawn between both simple ILs as a guide for the eye.

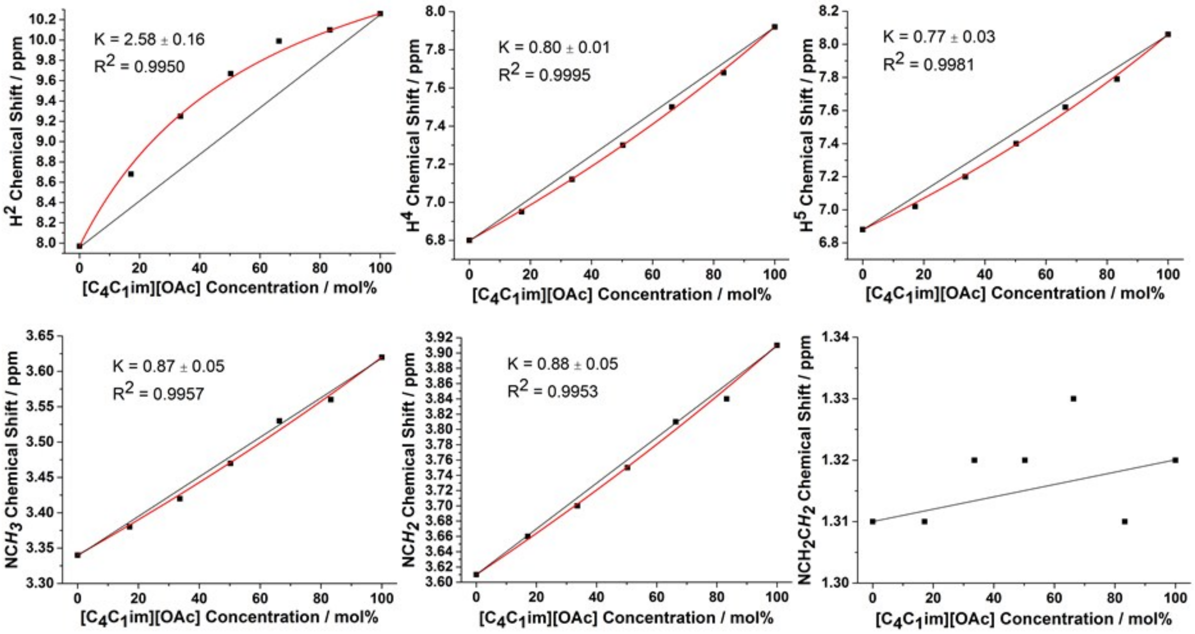

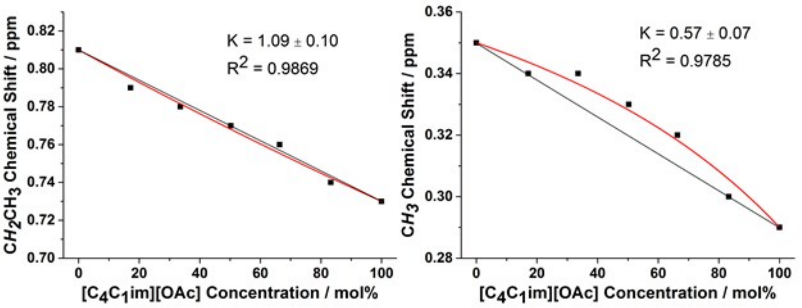

Fig. S28 ^{1}H NMR chemical shifts for different imidazolium cation shifts of $[C_4C_1im][OAc]_x[NTf_2]_{1-x}$ mixtures referenced to an internal capillary of DMSO-d_6. Red lines represent the fitted model with given fitting parameters where a reliable fit could be obtained, black lines are drawn between both simple ILs as a guide for the eye.

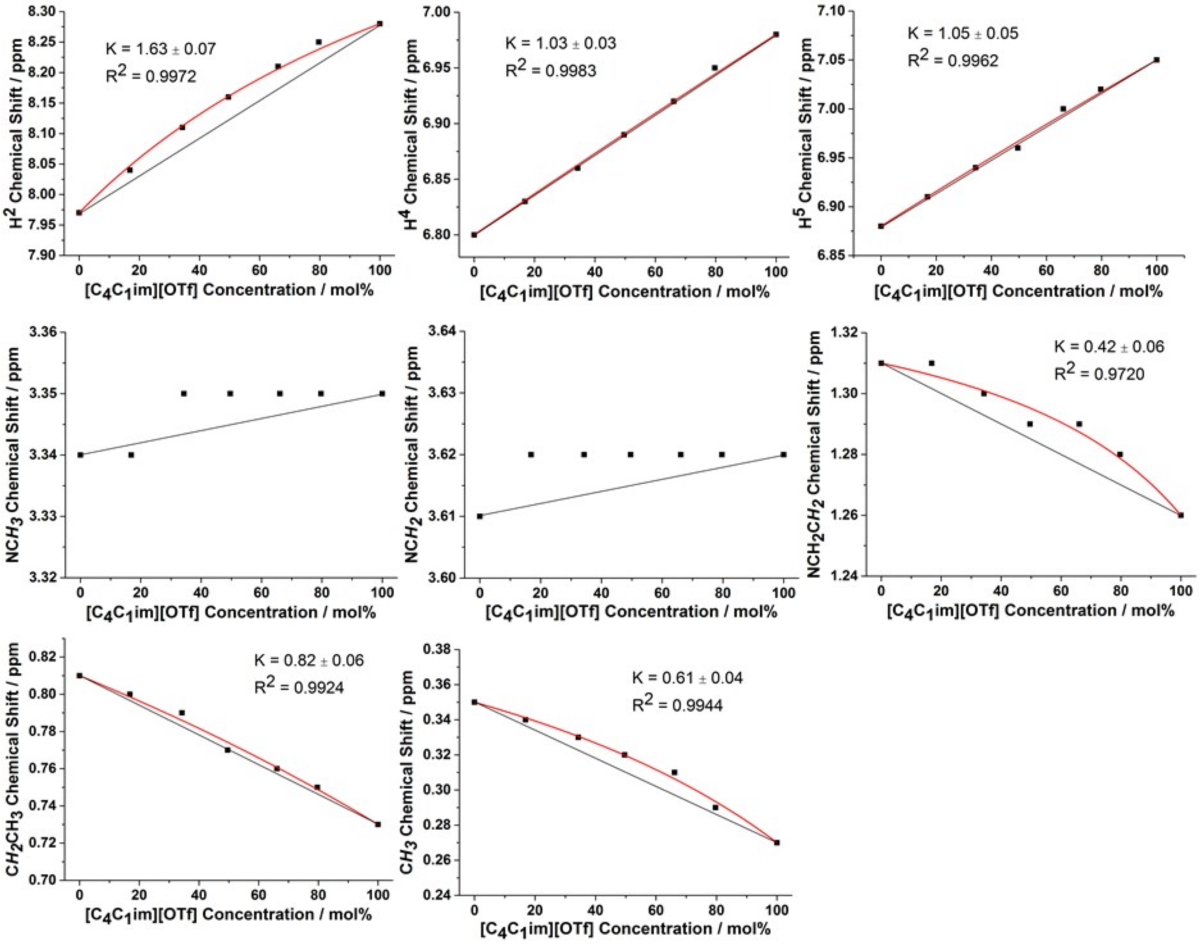

Fig. S29 ^{1}H NMR chemical shifts for different imidazolium cation shifts of $[C_4C_1im][OTf]_x[NTf_2]_{1-x}$ mixtures referenced to an internal capillary of DMSO-d_6. Red lines represent the fitted model with given fitting parameters where a reliable fit could be obtained, black lines are drawn between both simple ILs as a guide for the eye.

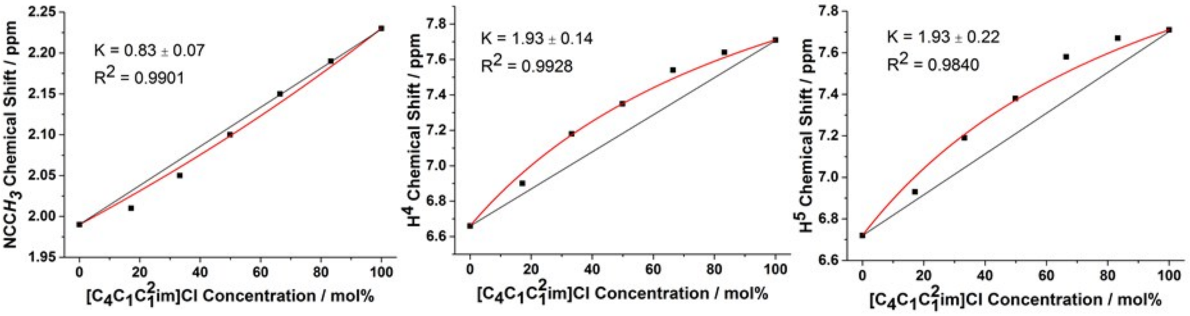

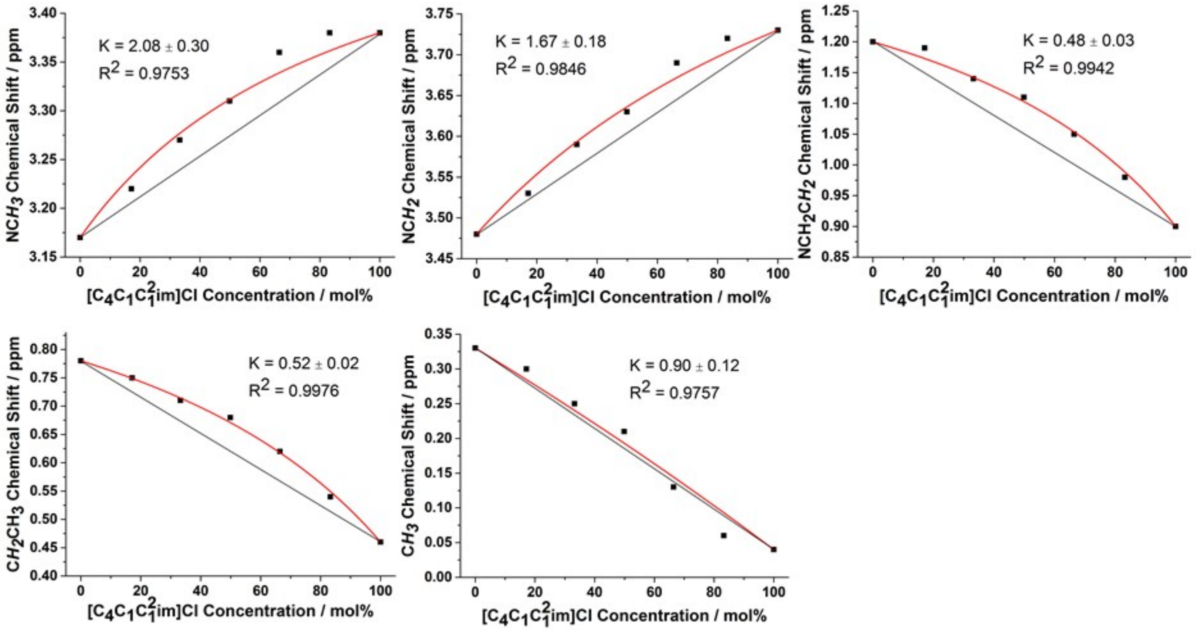

Fig. S30 ^{1}H NMR chemical shifts for different imidazolium cation shifts of $[C_4C_1C_1{}^2im]Cl_x[NTf_2]_{1-x}$ mixtures referenced to an internal capillary of DMSO-d_6. Red lines represent the fitted model with given fitting parameters, black lines are drawn between both simple ILs as a guide for the eye.

Table S28. ^{1}H NMR chemical shifts of undiluted ILs for $[C_4C_1im][Me_2PO_4]_x[NTf_2]_{1-x}$ mixtures.

x	H^2	H^4	H^5	NCH_3	NCH_2	NCH_2CH_2	CH_2CH_3	CH_3
0.00	7.98	6.81	6.89	3.35	3.63	1.33	0.82	0.37
0.17	8.52	6.93	7.01	3.38	3.66	1.32	0.8	0.35
0.33	8.93	7.06	7.15	3.41	3.69	1.32	0.78	0.33
0.50	9.25	7.22	7.32	3.43	3.72	1.3	0.75	0.31
0.67	9.45	7.38	7.5	3.46	3.75	1.29	0.73	0.28
0.83	9.58	7.53	7.68	3.49	3.78	1.27	0.7	0.26
1.00	9.68	7.67	7.84	3.51	3.8	1.26	0.67	0.23

Table S29. ^{1}H NMR chemical shifts of undiluted ILs for $[C_4C_1im]Cl_x[NTf_2]_{1-x}$ mixtures.

x	H^2	H^4	H^5	NCH_3	NCH_2	NCH_2CH_2	CH_2CH_3	CH_3
0.00	7.97	6.81	6.88	3.34	3.62	1.31	0.805	0.36
0.17	8.48	6.96	7.04	3.37	3.66	1.3	0.775	0.32
0.33	8.87	7.1	7.18	3.4	3.69	1.28	0.725	0.28
0.50	9.32	7.31	7.41	3.44	3.74	1.26	0.68	0.23
0.67	9.56	7.5	7.6	3.47	3.78	1.23	0.625	0.18
0.83	9.72	7.67	7.78	3.5	3.8	1.18	0.555	0.11
0.89	9.77	7.73	7.84	3.5	3.8	1.16	0.52	0.08
0.95	9.79	7.77	7.89	3.51	3.8	1.14	0.49	0.05
1.00	9.79	7.8	7.92	3.49	3.79	1.09	0.435	0.01

Table S30. ^{1}H NMR chemical shifts of undiluted ILs for $[C_4C_1im]Cl_x[OTf]_{1-x}$ mixtures.

x	H^2	H^4	H^5	NCH$_3$	NCH$_2$	NCH$_2$CH$_2$	CH$_2$CH$_3$	CH$_3$
0.00	8.28	6.97	7.05	3.35	3.62	1.26	0.72	0.27
0.17	8.65	7.12	7.19	3.38	3.66	1.25	0.695	0.24
0.33	9	7.27	7.35	3.4	3.7	1.23	0.65	0.2
0.50	9.27	7.42	7.51	3.43	3.73	1.21	0.61	0.16
0.67	9.44	7.52	7.62	3.45	3.75	1.18	0.57	0.12
0.83	9.61	7.65	7.76	3.47	3.77	1.14	0.505	0.06
1.00	9.805	7.815	7.935	3.505	3.8	1.1	0.4475	0.01

Table S31. ^{1}H NMR chemical shifts of undiluted ILs for $[C_4C_1im]Cl_x[SCN]_{1-x}$ mixtures.

x	H^2	H^4	H^5	NCH$_3$	NCH$_2$	NCH$_2$CH$_2$	CH$_2$CH$_3$	CH$_3$
0.00	8.58	7.17	7.23	3.47	3.73	1.28	0.705	0.24
0.17	8.84	7.26	7.32	3.47	3.74	1.25	0.67	0.21
0.33	9.06	7.35	7.42	3.47	3.75	1.23	0.63	0.17
0.50	9.26	7.45	7.52	3.47	3.75	1.2	0.585	0.13
0.67	9.49	7.58	7.67	3.48	3.77	1.16	0.535	0.09
0.83	9.64	7.68	7.79	3.49	3.78	1.13	0.49	0.04
1.00	9.805	7.815	7.935	3.505	3.8	1.1	0.4475	0.01

Table S32. ^{1}H NMR chemical shifts of undiluted ILs for $[C_4C_1im][OAc]_x[NTf_2]_{1-x}$ mixtures.

x	H^2	H^4	H^5	NCH$_3$	NCH$_2$	NCH$_2$CH$_2$	CH$_2$CH$_3$	CH$_3$
0.00	7.97	6.8	6.88	3.34	3.61	1.31	0.81	0.35
0.17	8.68	6.95	7.02	3.38	3.66	1.31	0.79	0.34
0.34	9.25	7.12	7.2	3.42	3.7	1.32	0.78	0.34
0.50	9.67	7.3	7.4	3.47	3.75	1.32	0.77	0.33
0.66	9.99	7.5	7.62	3.53	3.81	1.33	0.76	0.32
0.83	10.1	7.68	7.79	3.56	3.84	1.31	0.74	0.3
1.00	10.26	7.92	8.06	3.62	3.91	1.32	0.73	0.29

Table S33. ^{1}H NMR chemical shifts of undiluted ILs for $[C_4C_1im][OTf]_x[NTf_2]_{1-x}$ mixtures.

x	H^2	H^4	H^5	NCH$_3$	NCH$_2$	NCH$_2$CH$_2$	CH$_2$CH$_3$	CH$_3$
0.00	7.97	6.8	6.88	3.34	3.61	1.31	0.81	0.35
0.17	8.04	6.83	6.91	3.34	3.62	1.31	0.8	0.34
0.34	8.11	6.86	6.94	3.35	3.62	1.3	0.79	0.33
0.50	8.16	6.89	6.96	3.35	3.62	1.29	0.77	0.32
0.66	8.21	6.92	7	3.35	3.62	1.29	0.76	0.31
0.80	8.25	6.95	7.02	3.35	3.62	1.28	0.75	0.29
1.00	8.28	6.98	7.05	3.35	3.62	1.26	0.73	0.27

Table S34. ^{1}H NMR chemical shifts of undiluted ILs for $[C_4C_1C_1^2im]Cl_x[NTf_2]_{1-x}$ mixtures.

x	NCCH$_3$	H^4	H^5	NCH$_3$	NCH$_2$	NCH$_2$CH$_2$	CH$_2$CH$_3$	CH$_3$
0.00	1.99	6.66	6.72	3.17	3.48	1.2	0.78	0.33
0.17	2.01	6.9	6.93	3.22	3.53	1.19	0.75	0.3
0.33	2.05	7.18	7.19	3.27	3.59	1.14	0.71	0.25
0.50	2.1	7.35	7.38	3.31	3.63	1.11	0.68	0.21
0.66	2.15	7.54	7.58	3.36	3.69	1.05	0.62	0.13
0.83	2.19	7.64	7.67	3.38	3.72	0.98	0.54	0.06
1.00	2.23	7.71	7.71	3.38	3.73	0.9	0.46	0.04

^{13}C NMR Experiments

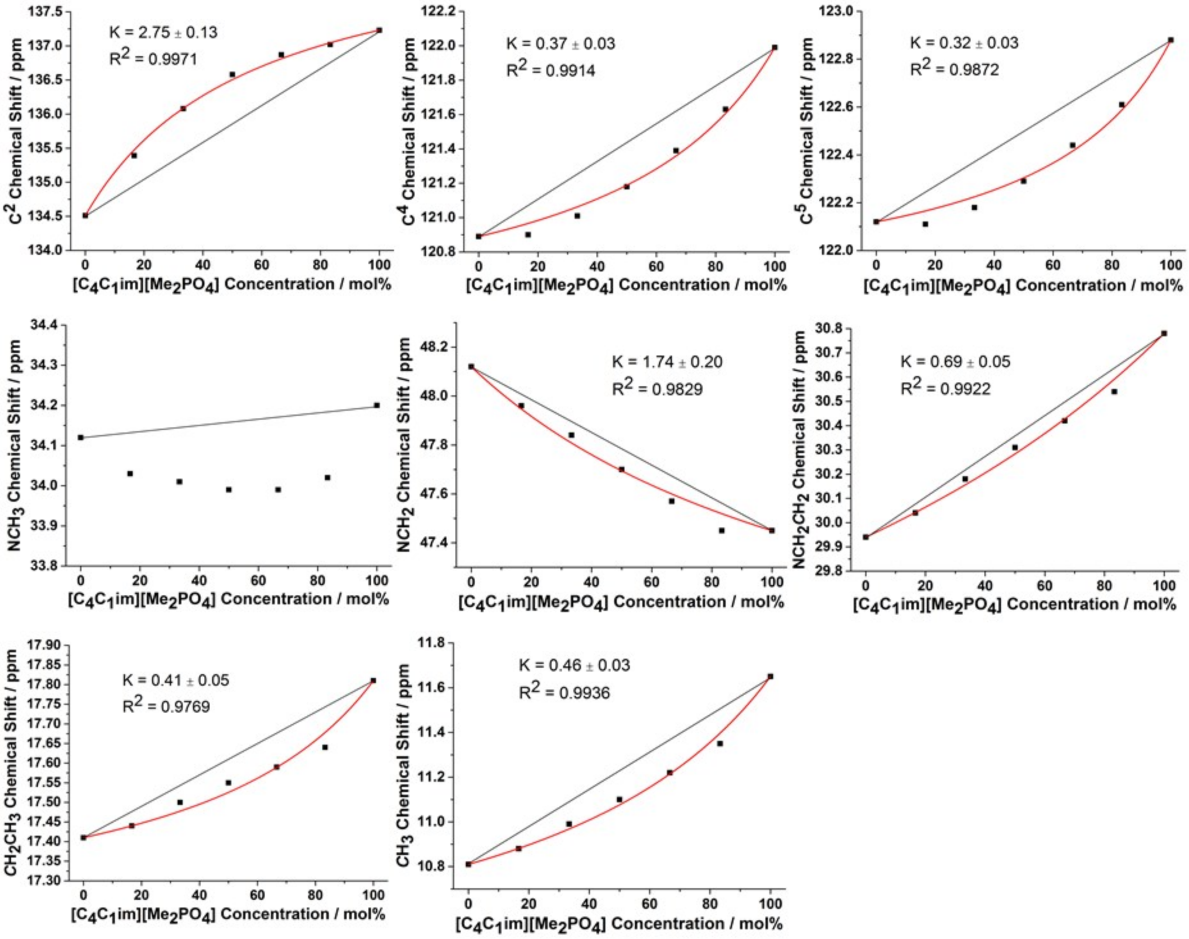

Fig. S31 ^{13}C NMR chemical shifts for different imidazolium cation shifts of $[C_4C_1im][Me_2PO_4]_x[NTf_2]_{1-x}$ mixtures referenced to an internal capillary of DMSO-d_6. Red lines represent the fitted model with given fitting parameters where a reliable fit could be obtained, black lines are drawn between both simple ILs as a guide for the eye.

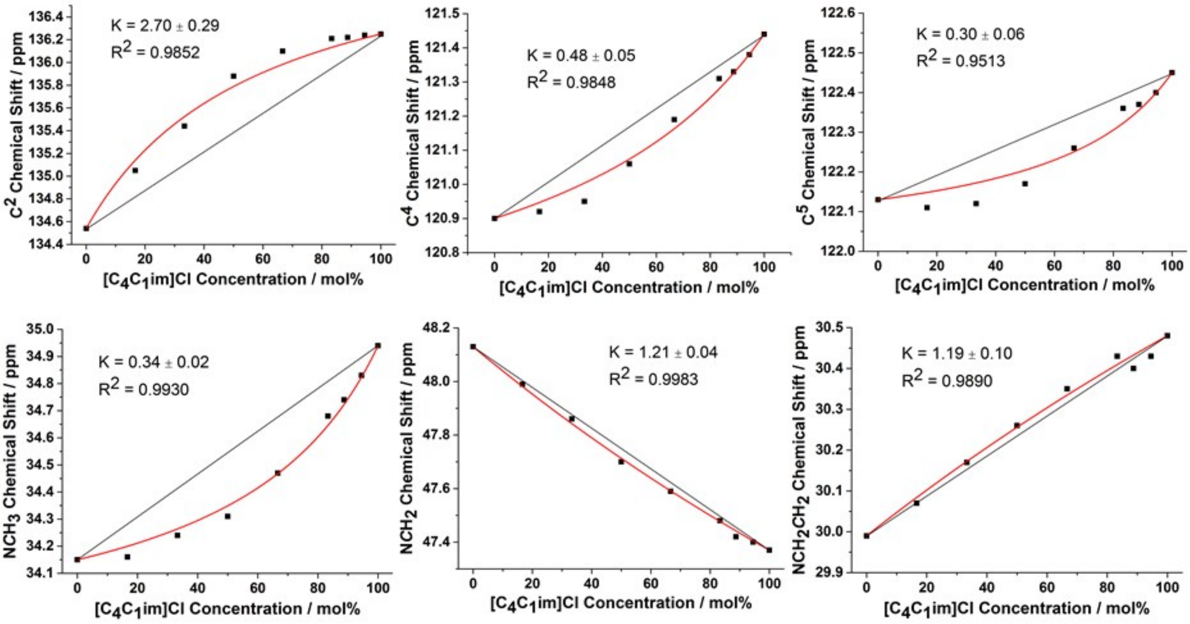

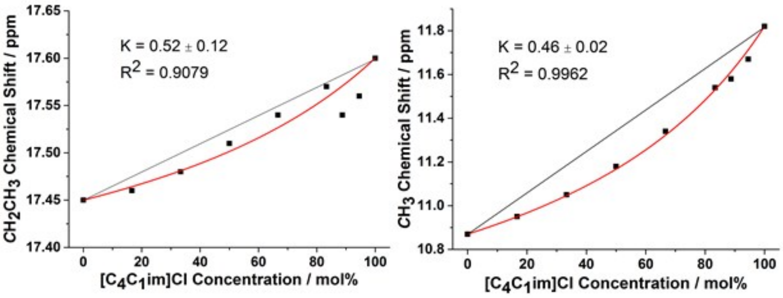

Fig. S32 ^{13}C NMR chemical shifts for different imidazolium cation shifts of $[C_4C_1im]Cl_x[NTf_2]_{1-x}$ mixtures referenced to an internal capillary of DMSO-d_6. Red lines represent the fitted model with given fitting parameters, black lines are drawn between both simple ILs as a guide for the eye.

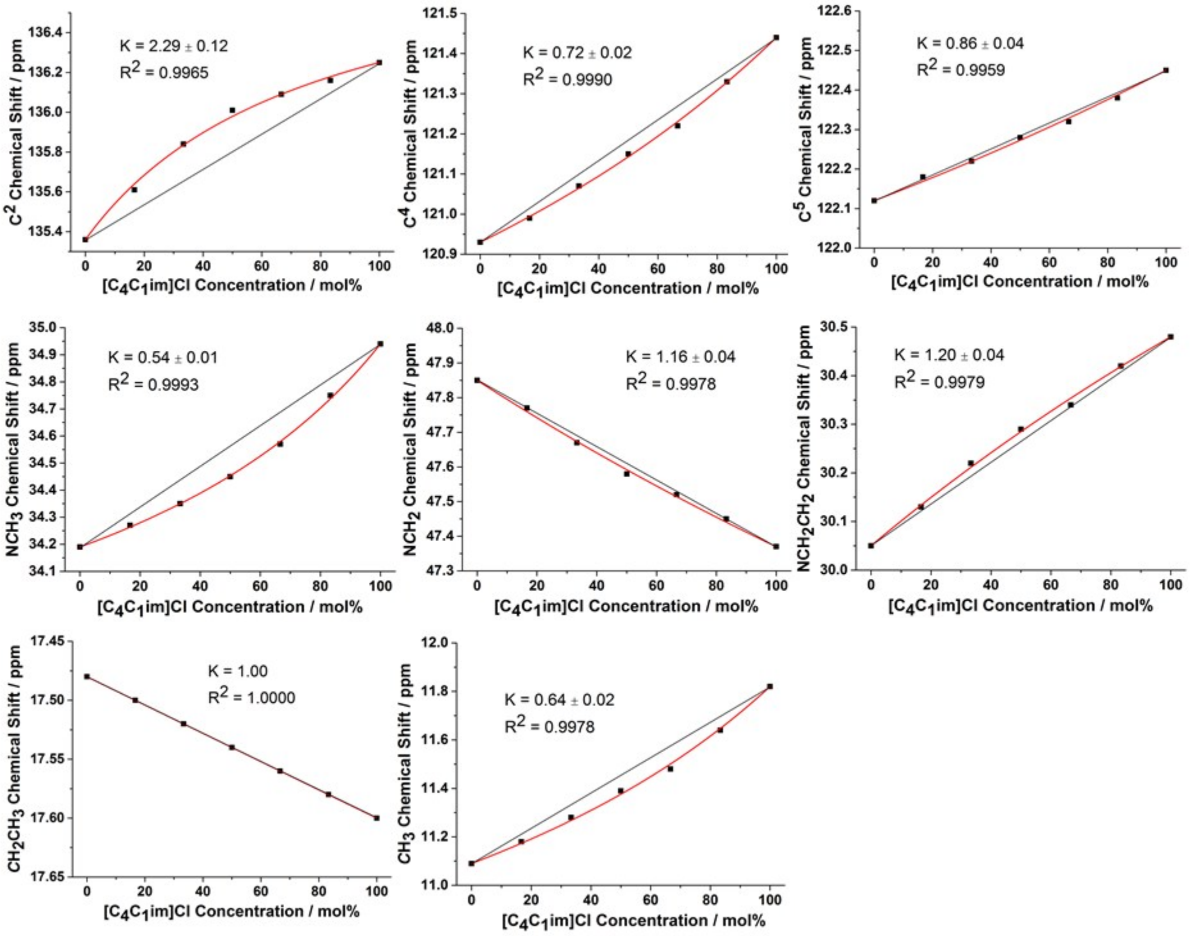

Fig. S33 ^{13}C NMR chemical shifts for different imidazolium cation shifts of $[C_4C_1im]Cl_x[OTf]_{1-x}$ mixtures referenced to an internal capillary of DMSO-d_6. Red lines represent the fitted model with given fitting parameters, black lines are drawn between both simple ILs as a guide for the eye.

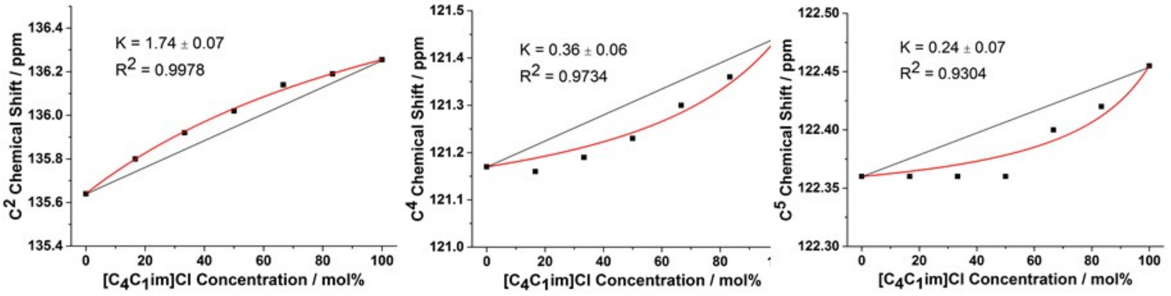

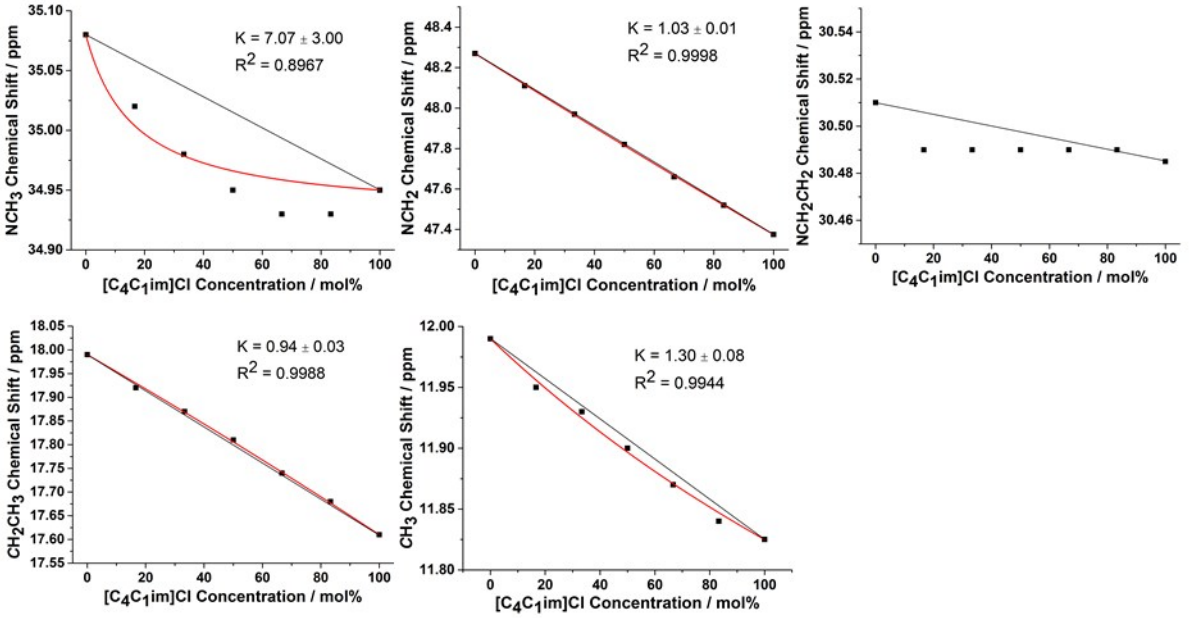

Fig. S34 ^{13}C NMR chemical shifts for different imidazolium cation shifts of $[C_4C_1im]Cl_x[SCN]_{1-x}$ mixtures referenced to an internal capillary of DMSO-*d*$_6$. Red lines represent the fitted model with given fitting parameters where a reliable fit could be obtained, black lines are drawn between both simple ILs as a guide for the eye.

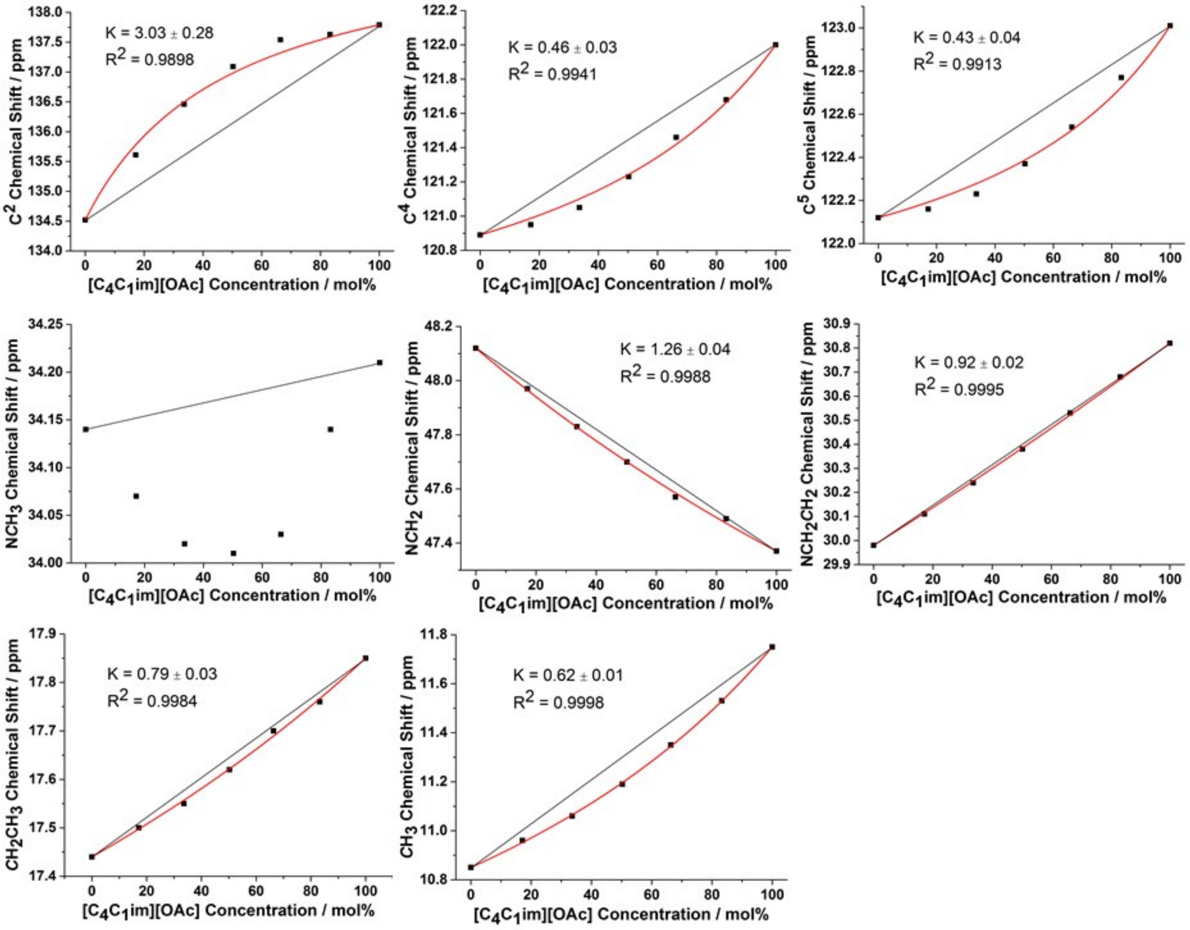

Fig. S35 ^{13}C NMR chemical shifts for different imidazolium cation shifts of $[C_4C_1im][OAc]_x[NTf_2]_{1-x}$ mixtures referenced to an internal capillary of DMSO-*d*$_6$. Red lines represent the fitted model with given fitting parameters where a reliable fit could be obtained, black lines are drawn between both simple ILs as a guide for the eye.

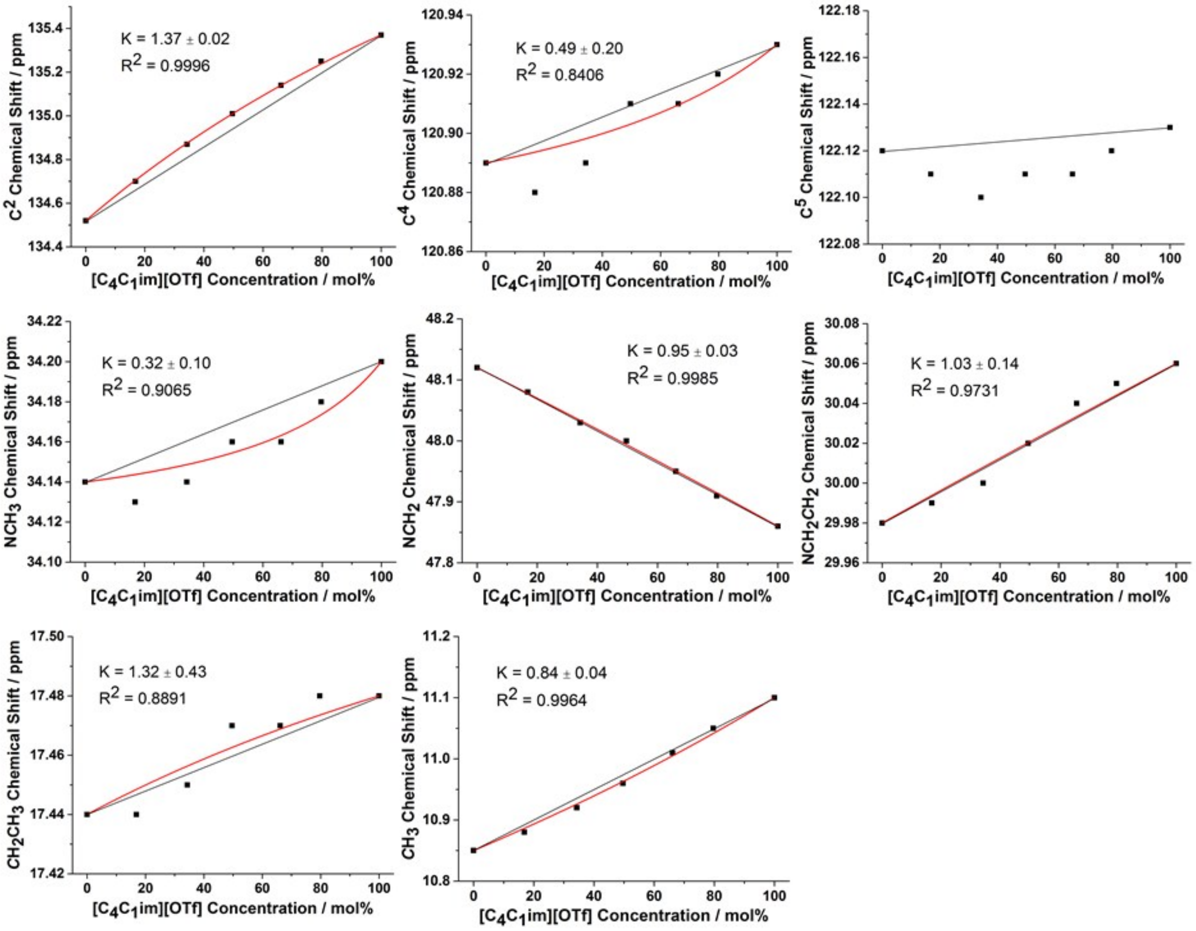

Fig. S36 ^{13}C NMR chemical shifts for different imidazolium cation shifts of [C$_4$C$_1$im][OTf]$_x$[NTf$_2$]$_{1-x}$ mixtures referenced to an internal capillary of DMSO-*d*$_6$. Red lines represent the fitted model with given fitting parameters where a reliable fit could be obtained, black lines are drawn between both simple ILs as a guide for the eye.

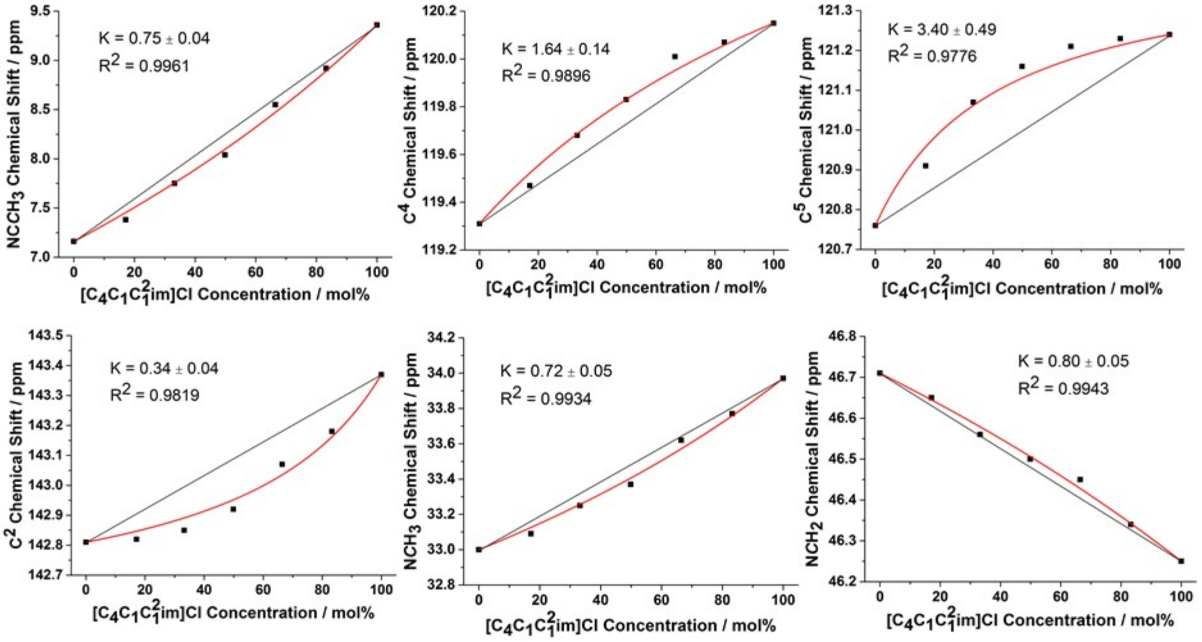

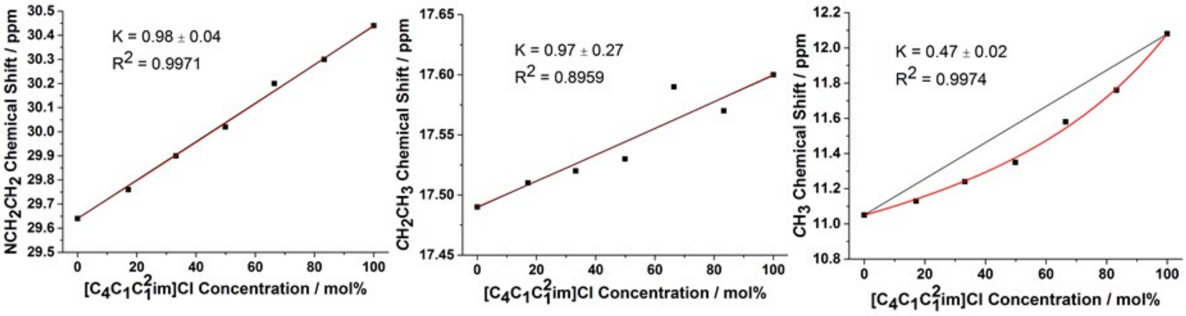

Fig. S37 ^{13}C NMR chemical shifts for different imidazolium cation shifts of $[C_4C_1C_1^2im]Cl_x[NTf_2]_{1-x}$ mixtures referenced to an internal capillary of DMSO-*d*$_6$. Red lines represent the fitted model with given fitting parameters, black lines are drawn between both simple ILs as a guide for the eye.

Table S35. ^{13}C NMR chemical shifts of undiluted ILs for $[C_4C_1im][Me_2PO_4]_x[NTf_2]_{1-x}$ mixtures.

x	C^2	C^4	C^5	NCH$_3$	NCH$_2$	NCH$_2$CH$_2$	CH$_2$CH$_3$	CH$_3$
0.00	134.51	120.89	122.12	34.12	48.12	29.94	17.41	10.81
0.17	135.39	120.9	122.11	34.03	47.96	30.04	17.44	10.88
0.33	136.08	121.01	122.18	34.01	47.84	30.18	17.5	10.99
0.50	136.58	121.18	122.29	33.99	47.7	30.31	17.55	11.1
0.67	136.87	121.39	122.44	33.99	47.57	30.42	17.59	11.22
0.83	137.02	121.63	122.61	34.02	47.45	30.54	17.64	11.35
1.00	137.23	121.99	122.88	34.2	47.45	30.78	17.81	11.65

Table S36. ^{13}C NMR chemical shifts of undiluted ILs for $[C_4C_1im]Cl_x[NTf_2]_{1-x}$ mixtures.

x	C^2	C^4	C^5	NCH$_3$	NCH$_2$	NCH$_2$CH$_2$	CH$_2$CH$_3$	CH$_3$
0.00	134.54	120.9	122.13	34.15	48.13	29.99	17.45	10.87
0.17	135.05	120.92	122.11	34.16	47.99	30.07	17.46	10.95
0.33	135.44	120.95	122.12	34.24	47.86	30.17	17.48	11.05
0.50	135.88	121.06	122.17	34.31	47.7	30.26	17.51	11.18
0.67	136.1	121.19	122.26	34.47	47.59	30.35	17.54	11.34
0.83	136.21	121.31	122.36	34.68	47.48	30.43	17.57	11.54
0.89	136.22	121.33	122.37	34.74	47.42	30.4	17.54	11.58
0.95	136.24	121.38	122.4	34.83	47.4	30.43	17.56	11.67
1.00	136.25	121.44	122.45	34.94	47.37	30.48	17.6	11.82

Table S37. ^{13}C NMR chemical shifts of undiluted ILs for $[C_4C_1im]Cl_x[OTf]_{1-x}$ mixtures.

x	C^2	C^4	C^5	NCH$_3$	NCH$_2$	NCH$_2$CH$_2$	CH$_2$CH$_3$	CH$_3$
0.00	135.36	120.93	122.12	34.19	47.85	30.05	17.48	11.09
0.17	135.61	120.99	122.18	34.27	47.77	30.13	17.5	11.18
0.33	135.84	121.07	122.22	34.35	47.67	30.22	17.52	11.28
0.50	136.01	121.15	122.28	34.45	47.58	30.29	17.54	11.39
0.67	136.09	121.22	122.32	34.57	47.52	30.34	17.56	11.48
0.83	136.16	121.33	122.38	34.75	47.45	30.42	17.58	11.64
1.00	136.25	121.44	122.45	34.94	47.37	30.48	17.6	11.82

Table S38. ^{13}C NMR chemical shifts of undiluted ILs for $[C_4C_1im]Cl_x[SCN]_{1-x}$ mixtures.

x	C^2	C^4	C^5	NCH$_3$	NCH$_2$	NCH$_2$CH$_2$	CH$_2$CH$_3$	CH$_3$
0.00	135.64	121.17	122.36	35.08	48.27	30.51	17.99	11.99
0.17	135.8	121.16	122.36	35.02	48.11	30.49	17.92	11.95
0.33	135.92	121.19	122.36	34.98	47.97	30.49	17.87	11.93
0.50	136.02	121.23	122.36	34.95	47.82	30.49	17.81	11.9
0.67	136.14	121.3	122.4	34.93	47.66	30.49	17.74	11.87
0.83	136.19	121.36	122.42	34.93	47.52	30.49	17.68	11.84
1.00	136.255	121.445	122.455	34.95	47.375	30.485	17.61	11.825

Table S39. ^{13}C NMR chemical shifts of undiluted ILs for $[C_4C_1im][OAc]_x[NTf_2]_{1-x}$ mixtures.

x	C^2	C^4	C^5	NCH$_3$	NCH$_2$	NCH$_2$CH$_2$	CH$_2$CH$_3$	CH$_3$
0.00	134.52	120.89	122.12	34.14	48.12	29.98	17.44	10.85
0.17	135.61	120.95	122.16	34.07	47.97	30.11	17.5	10.96
0.34	136.46	121.05	122.23	34.02	47.83	30.24	17.55	11.06
0.50	137.09	121.23	122.37	34.01	47.7	30.38	17.62	11.19
0.66	137.54	121.46	122.54	34.03	47.57	30.53	17.7	11.35
0.83	137.63	121.68	122.77	34.14	47.49	30.68	17.76	11.53
1.00	137.79	122	123.01	34.21	47.37	30.82	17.85	11.75

Table S40. ^{13}C NMR chemical shifts of undiluted ILs for $[C_4C_1im][OTf]_x[NTf_2]_{1-x}$ mixtures.

x	C^2	C^4	C^5	NCH$_3$	NCH$_2$	NCH$_2$CH$_2$	CH$_2$CH$_3$	CH$_3$
0.00	134.52	120.89	122.12	34.14	48.12	29.98	17.44	10.85
0.17	134.7	120.88	122.11	34.13	48.08	29.99	17.44	10.88
0.34	134.87	120.89	122.1	34.14	48.03	30	17.45	10.92
0.50	135.01	120.91	122.11	34.16	48	30.02	17.47	10.96
0.66	135.14	120.91	122.11	34.16	47.95	30.04	17.47	11.01
0.80	135.25	120.92	122.12	34.18	47.91	30.05	17.48	11.05
1.00	135.37	120.93	122.13	34.2	47.86	30.06	17.48	11.1

Table S41. ^{13}C NMR chemical shifts of undiluted ILs for $[C_4C_1C_1{}^2im]Cl_x[NTf_2]_{1-x}$ mixtures.

x	NCCH$_3$	C^4	C^5	C^2	NCH$_3$	NCH$_2$	NCH$_2$CH$_2$	CH$_2$CH$_3$	CH$_3$
0.00	7.16	119.31	120.76	142.81	33	46.71	29.64	17.49	11.05
0.17	7.38	119.47	120.91	142.82	33.09	46.65	29.76	17.51	11.13
0.33	7.75	119.68	121.07	142.85	33.25	46.56	29.9	17.52	11.24
0.50	8.04	119.83	121.16	142.92	33.37	46.5	30.02	17.53	11.35
0.66	8.55	120.01	121.21	143.07	33.62	46.45	30.2	17.59	11.58
0.83	8.92	120.07	121.23	143.18	33.77	46.34	30.3	17.57	11.76
1.00	9.36	120.15	121.24	143.37	33.97	46.25	30.44	17.6	12.08

Table S42. Compilation of Δβ values for each of the IL mixtures studied.

Ionic Liquid Mixture	Δβ
$[C_4C_1im][Me_2PO_4]_x[NTf_2]_{1-x}$	0.9[14]
$[C_4C_1im]Cl_x[NTf_2]_{1-x}$	0.72[14, 31]
$[C_4C_1im]Cl_x[OTf]_{1-x}$	0.46[14, 31]
$[C_4C_1im]Cl_x[SCN]_{1-x}$	0.24[31]
$[C_4C_1im][OAc]_x[NTf_2]_{1-x}$	0.97[14]
$[C_4C_1im][OTf]_x[NTf_2]_{1-x}$	0.26[14]

Undiluted [C_4C_1im][C_4C_1pyrr] Mixture NMR Experiments

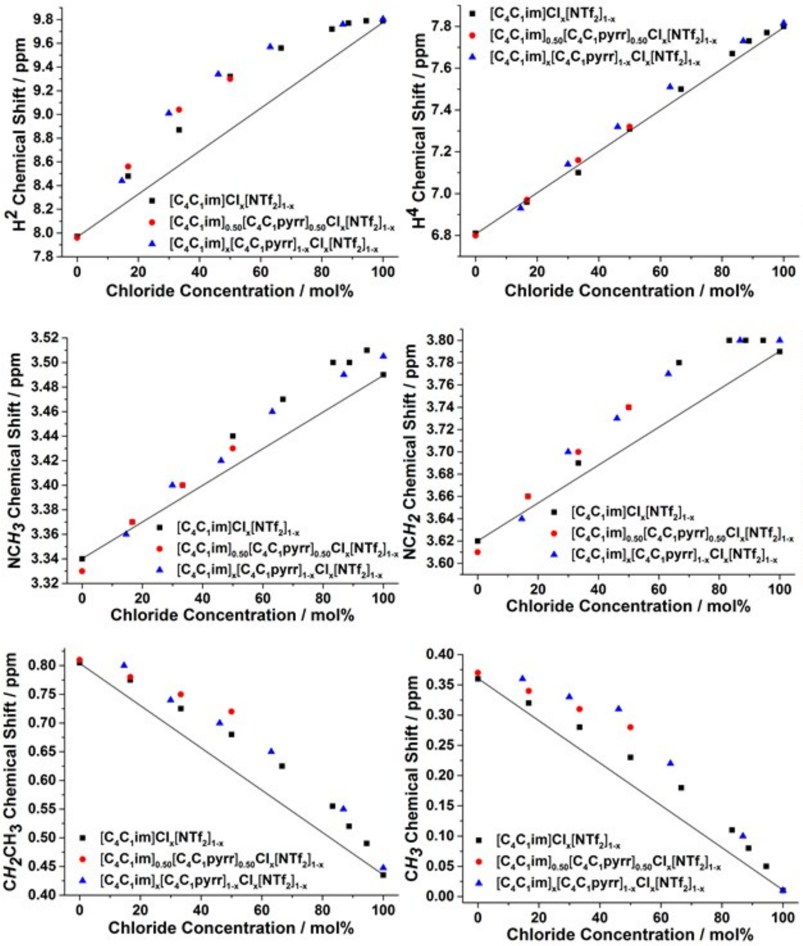

Fig. S38 ^{1}H NMR chemical shifts of the [C_4C_1im]$^+$ cation in [C_4C_1im]$Cl_x[NTf_2]_{1-x}$ (black square), [C_4C_1im]$_{0.50}$[C_4C_1pyrr]$_{0.50}Cl_x[NTf_2]_{1-x}$ (red circle) and [C_4C_1im]$_x$[C_4C_1pyrr]$_{1-x}Cl_x[NTf_2]_{1-x}$ (blue triangle) mixtures referenced internally to DMSO-d_6 as a function of the chloride ratio. Black lines are drawn between simple [C_4C_1im][NTf_2] and [C_4C_1im]Cl as a guide for the eye.

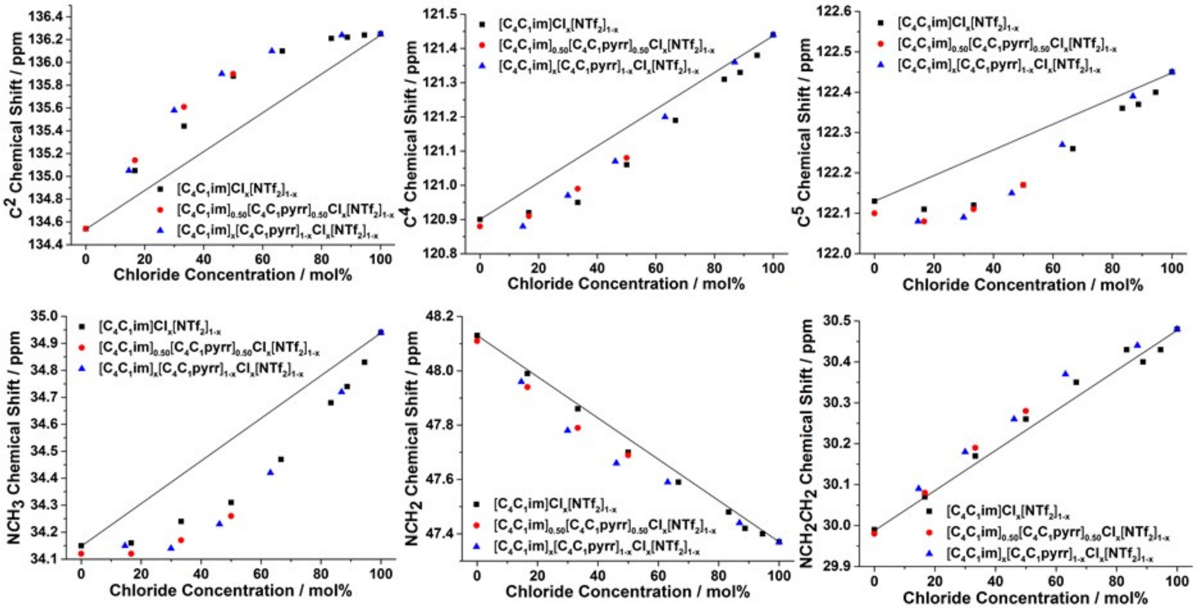

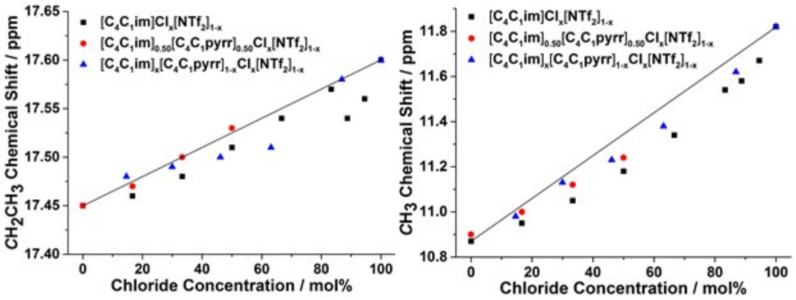

Fig. S39 ^{13}C NMR chemical shifts of the $[C_4C_1Im]^+$ cation in $[C_4C_1im]Cl_x[NTf_2]_{1-x}$ (black square), $[C_4C_1im]_{0.50}[C_4C_1pyrr]_{0.50}Cl_x[NTf_2]_{1-x}$ (red circle) and $[C_4C_1im]_x[C_4C_1pyrr]_{1-x}Cl_x[NTf_2]_{1-x}$ (blue triangle) mixtures referenced internally to DMSO-d_6 as a function of the chloride ratio. Black lines are drawn between simple $[C_4C_1im][NTf_2]$ and $[C_4C_1im]Cl$ as a guide for the eye.

Table S43. ^1H NMR chemical shifts for the $[C_4C_1im]^+$ cation of undiluted ILs for $[C_4C_1im]_{0.50}[C_4C_1pyrr]_{0.50}Cl_x[NTf_2]_{1-x}$ mixtures.

x	H^2	H^4	H^5	NCH_3	NCH_2	NCH_2CH_2	CH_2CH_3	CH_3
0.00	7.96	6.8	6.87	3.33	3.61	1.31	0.81	0.37
0.17	8.56	6.97	7.06	3.37	3.66	1.3	0.78	0.34
0.33	9.04	7.16	7.25	3.4	3.7	1.29	0.75	0.31
0.50	9.3	7.32	7.42	3.43	3.74	1.27	0.72	0.28

Table S44. ^1H NMR chemical shifts for the $[C_4C_1im]^+$ cation of undiluted ILs for $[C_4C_1im]_x[C_4C_1pyrr]_{1-x}Cl_x[NTf_2]_{1-x}$ mixtures.

x	H^2	H^4	H^5	NCH_3	NCH_2	NCH_2CH_2	CH_2CH_3	CH_3
0.15	8.44	6.93	7	3.36	3.64	1.3	0.8	0.36
0.30	9.01	7.14	7.24	3.4	3.7	1.29	0.74	0.33
0.46	9.34	7.32	7.43	3.42	3.73	1.26	0.7	0.31
0.63	9.57	7.51	7.61	3.46	3.77	1.24	0.65	0.22
0.87	9.76	7.73	7.84	3.49	3.8	1.17	0.55	0.1
1.00	9.805	7.815	7.935	3.505	3.8	1.1	0.4475	0.01

Table S45. ^{13}C NMR chemical shifts for the $[C_4C_1im]^+$ cation of undiluted ILs for $[C_4C_1im]_{0.50}[C_4C_1pyrr]_{0.50}Cl_x[NTf_2]_{1-x}$ mixtures.

x	C^2	C^4	C^5	NCH_3	NCH_2	NCH_2CH_2	CH_2CH_3	CH_3
0.00	134.54	120.88	122.1	34.12	48.11	29.98	17.45	10.9
0.17	135.14	120.91	122.08	34.12	47.94	30.08	17.47	11
0.33	135.61	120.99	122.11	34.17	47.79	30.19	17.5	11.12
0.50	135.9	121.08	122.17	34.26	47.69	30.28	17.53	11.24

Table S46. ^{13}C NMR chemical shifts for the $[C_4C_1im]^+$ cation of undiluted ILs for $[C_4C_1im]_x[C_4C_1pyrr]_{1-x}Cl_x[NTf_2]_{1-x}$ mixtures.

x	C^2	C^4	C^5	NCH_3	NCH_2	NCH_2CH_2	CH_2CH_3	CH_3
0.15	135.05	120.88	122.08	34.15	47.96	30.09	17.48	10.98
0.30	135.58	120.97	122.09	34.14	47.78	30.18	17.49	11.13
0.46	135.9	121.07	122.15	34.23	47.66	30.26	17.5	11.23
0.63	136.1	121.2	122.27	34.42	47.59	30.37	17.51	11.38
0.87	136.24	121.36	122.39	34.72	47.44	30.44	17.58	11.62
1.00	136.25	121.44	122.45	34.94	47.37	30.48	17.6	11.82

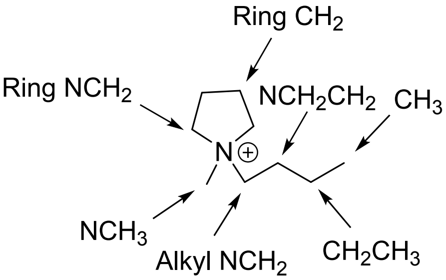

Fig. S40 The different atomic positions on the $[C_4C_1pyrr]^+$ cation, labelled as they will be referred to in this article.

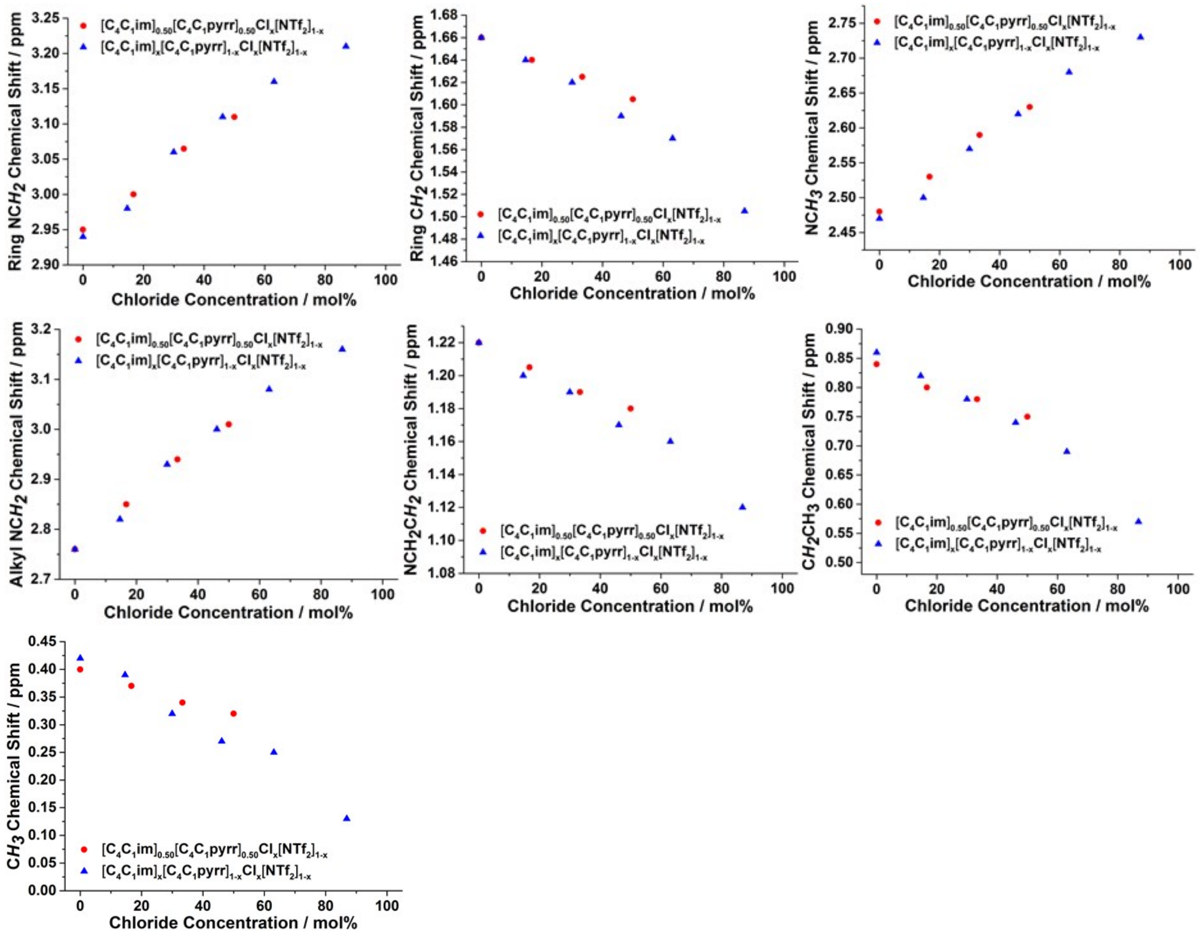

Fig. S41 ^{1}H NMR chemical shifts of the $[C_4C_1pyrr]^+$ cation in $[C_4C_1im]_{0.50}[C_4C_1pyrr]_{0.50}Cl_x[NTf_2]_{1-x}$ (red circle) and $[C_4C_1im]_x[C_4C_1pyrr]_{1-x}Cl_x[NTf_2]_{1-x}$ (blue triangle) mixtures referenced internally to DMSO-d_6 as a function of the chloride ratio. The high melting point of $[C_4C_1pyrr]Cl$ precluded its measurement.

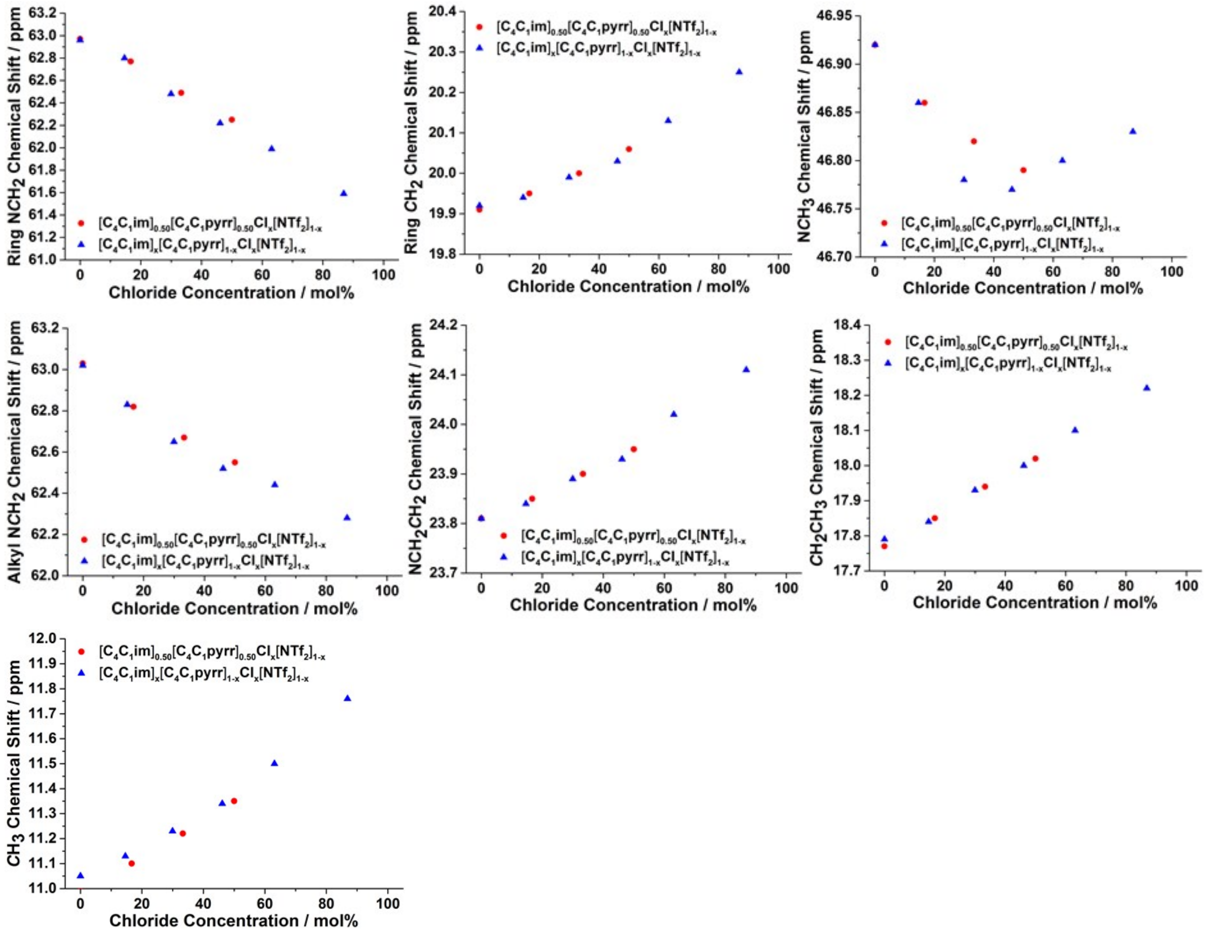

Fig. S42 ^{13}C NMR chemical shifts of the $[C_4C_1pyrr]^+$ cation in $[C_4C_1im]_{0.50}[C_4C_1pyrr]_{0.50}Cl_x[NTf_2]_{1-x}$ (red circle) and $[C_4C_1im]_x[C_4C_1pyrr]_{1-x}Cl_x[NTf_2]_{1-x}$ (blue triangle) mixtures referenced internally to DMSO-d_6 as a function of the chloride ratio. The high melting point of $[C_4C_1pyrr]Cl$ precluded its measurement.

Table S47. ^{1}H NMR chemical shifts for the $[C_4C_1pyrr]^+$ cation of undiluted ILs for $[C_4C_1im]_{0.50}[C_4C_1pyrr]_{0.50}Cl_x[NTf_2]_{1-x}$ mixtures.

x	Ring NCH$_2$	Ring CH$_2$	NCH$_3$	Alkyl NCH$_2$	NCH$_2$CH$_2$	CH$_2$CH$_3$	CH$_3$
0.00	2.95	1.66	2.48	2.76	1.22	0.84	0.4
0.17	3	1.64	2.53	2.85	1.205	0.8	0.37
0.33	3.065	1.625	2.59	2.94	1.19	0.78	0.34
0.50	3.11	1.605	2.63	3.01	1.18	0.75	0.32

Table S48. ^{1}H NMR chemical shifts for the $[C_4C_1pyrr]^+$ cation of undiluted ILs for $[C_4C_1im]_x[C_4C_1pyrr]_{1-x}Cl_x[NTf_2]_{1-x}$ mixtures.

x	Ring NCH$_2$	Ring CH$_2$	NCH$_3$	Alkyl NCH$_2$	NCH$_2$CH$_2$	CH$_2$CH$_3$	CH$_3$
0.00	2.94	1.66	2.47	2.76	1.22	0.86	0.42
0.15	2.98	1.64	2.5	2.82	1.2	0.82	0.39
0.30	3.06	1.62	2.57	2.93	1.19	0.78	0.32
0.46	3.11	1.59	2.62	3	1.17	0.74	0.27
0.63	3.16	1.57	2.68	3.08	1.16	0.69	0.25
0.87	3.21	1.505	2.73	3.16	1.12	0.57	0.13

Table S49. ^{13}C NMR chemical shifts for the $[C_4C_1pyrr]^+$ cation of undiluted ILs for $[C_4C_1im]_{0.50}[C_4C_1pyrr]_{0.50}Cl_x[NTf_2]_{1-x}$ mixtures.

x	Ring NCH$_2$	Ring CH$_2$	NCH$_3$	Alkyl NCH$_2$	NCH$_2$CH$_2$	CH$_2$CH$_3$	CH$_3$
0.00	63.03	23.81	46.92	62.97	19.91	17.77	10.99
0.17	62.82	23.85	46.86	62.77	19.95	17.85	11.1
0.33	62.67	23.9	46.82	62.49	20	17.94	11.22
0.50	62.55	23.95	46.79	62.25	20.06	18.02	11.35

Table S50. ^{13}C NMR chemical shifts for the $[C_4C_1pyrr]^+$ cation of undiluted ILs for $[C_4C_1im]_x[C_4C_1pyrr]_{1-x}Cl_x[NTf_2]_{1-x}$ mixtures.

x	Ring NCH$_2$	Ring CH$_2$	NCH$_3$	Alkyl NCH$_2$	NCH$_2$CH$_2$	CH$_2$CH$_3$	CH$_3$
0.00	63.02	23.81	46.92	62.96	19.92	17.79	11.05
0.15	62.83	23.84	46.86	62.8	19.94	17.84	11.13
0.30	62.65	23.89	46.78	62.48	19.99	17.93	11.23
0.46	62.52	23.93	46.77	62.22	20.03	18	11.34
0.63	62.44	24.02	46.8	61.99	20.13	18.1	11.5
0.87	62.28	24.11	46.83	61.59	20.25	18.22	11.76

Underlying Assumptions and Limitations of the NMR Model

There are a number of important assumptions and limitations to the NMR model used. First, this model cannot account for chemical shifts that lie outside of those of the simple ILs. As established from Figure 2 and Section D of the ESI, the majority of chemical shifts for the mixtures lie within the range defined by the simple IL constituents, with a minority of mixtures resulting in small deviations outside of this range. The model also assumes that the chemical shift can be described as an equilibrium between the local structure of the two simple ILs at a given cation environment and therefore is not able to account for features which do not appear in either of these two extremes, such as a bifurcated H-bond between both anions (A_1 and A_2) for example. Finally, it is important to emphasise that the model does not directly ascertain whether there is an actual interaction of the anion with a specific atom, only the extent to which the average local structure of that site over the population of cations is like either of the simple ILs. For example, it would be unlikely that the anion would interact directly with the terminal CH_3 on the butyl chain, however secondary structural and electronic effects would differ depending on the anion which could lead to a chemical shift change. This model therefore would consider the extent to which these secondary effects varied for the CH_3 group in the mixture relative to the proportion of anions in the mixture.

Another potential concern about the validity of such a model is that in a neat IL system the total concentration of anions A_1 and A_2 is equivalent to the concentration of C_i, in contrast to mixed solvent solvatochromic dye systems where the solvent is in vast excess. It could be envisaged that the chemical shift could saturate at low relative proportions of either anion if there was a very strong preference for the interaction of that anion with a given cation position. This would lead to an underestimated K value as the apparent proportion of interactions with one of the anions is artificially reduced. However, even if the conservative assumption is made that each anion could interact with no more than two cations, this limit is not reached for any system. Removal of the points with the lowest anion ratios also does not change the fitted values within experimental error, indicating this is not an issue for these mixtures and the fitted values of K are realistic.

Despite the simplicity of the model and its inherent assumptions, most of the NMR data is well modelled using this approach. The model did not provide a good fit for the chemical environments of the mixtures where there was either a small absolute chemical shift difference between the simple ILs or a chemical shift outside the range defined by the simple ILs was observed. The latter was obtained for the NCH_2 and NCH_3 ^1H signals of $[C_4C_1im]Cl_x[NTf_2]_{1-x}$, NCH_3 ^{13}C signal of $[C_4C_1im][Me_2PO_4]_x[NTf_2]_{1-x}$, NCH_3 ^{13}C signal of $[C_4C_1im]Cl_x[SCN]_{1-x}$ and the NCH_3 ^{13}C signal of $[C_4C_1im][OAc]_x[NTf_2]_{1-x}$. It is unlikely to be a coincidence that this model appears to fail only for some NCH_3 and NCH_2 signals. Compared to the imidazolium ring protons these groups have more conformational flexibility and are free to rotate. Additionally, they possess multiple hydrogen atoms and, as they are adjacent to the positively charged ring, they are capable of being involved in H-bonding interactions.[32] These factors mean that the hydrogen atoms in these positions can engage simultaneously in H-bonds with anions that are close to in plane with the imidazolium cation and those positioned above the imidazolium ring. This combination means that these interactions and the conformations adopted are not necessarily equivalent to those in either of the simple ILs, leading to a breakdown of the model.

Derivation of Anion Excess Equation and Underlying Assumptions

From consideration of the equilibrium constant, K, in Equation 1, and the anion mass balance, the relationship between the mole fraction of each anion interacting with cation site C_i (C_iA_1 and C_iA_2) can be derived in terms of K and the overall mole fraction of anions A_1 and A_2 in the system (M_{A1} and M_{A2} respectively) and is given by Equation S1.

$$x_{CiA1} = \frac{M_{A1}x_{CiA2}}{KM_{A2} + (1-K)x_{CiA2}}$$

Equation S1. Relationship between x_{CiA1} and x_{CiA2} in terms of known quantities.

It is then useful to define a mole fraction of interacting anions, X_{CA}, which is equivalent to the sum of x_{CiA1} and x_{CiA2}. This described the fraction of anions in the system directly interacting with a given cation location. Using the relationship in Equation S1, this value is then equivalent to that defined in Equation S2.

$$X_{CA} = \frac{(1-K)x_{CiA2}^2 + \left(M_{A1} + KM_{A2}\right)x_{CiA2}}{KM_{A2} + (1-K)x_{CiA2}}$$

Equation S2. Relationship between the total mole fraction of coordinated anions and x_{CiA2}.

Solving the quadratic equation that results from the rearrangement of Equation S2 allows for x_{CiA2} to be expressed in terms of the total mole fraction of coordinated anions (Equation S3).

$$x_{CiA2} = \frac{(1-K)X_{CA} - (M_{A1} + KM_{A2}) \pm \sqrt{((1-K)X_{CA} + M_{A1} + KM_{A2})^2 + 4KX_{CA}M_{A2}(1-K)}}{2(1-K)}$$

Equation S3. Analytical solution for x_{CiA2} in terms of X_{CA}.

From Equations S1 and S3, the fraction of A_1 or A_2 anions solvating the given cation site (F_{A1} and F_{A2} respectively), as defined by Equation S4, can be determined in terms of a single unknown quantity (X_{CA} or x_{CiA2}), Equation S5 and S6.

$$F_{A1} = \frac{x_{CiA1}}{x_{CiA1} + x_{CiA2}}$$

$$F_{A2} = \frac{x_{CiA2}}{x_{CiA1} + x_{CiA2}}$$

Equation S4. Mathematical definition of F_{A1} and F_{A2}.

$$F_{A1} = \frac{M_{A1}}{M_{A1} + KM_{A2} + (1 - K)x_{CiA2}}$$

$$F_{A2} = \frac{KM_{A2} + (1 - K)x_{CiA2}}{M_{A1} + KM_{A2} + (1 - K)x_{CiA2}}$$

Equation S5. F_{A1} and F_{A2} in terms of x_{CiA2}.

$$F_{A1} = \frac{2M_{A1}}{M_{A1} + KM_{A2} + X_{CA}(1 - K) \pm \sqrt{((1 - K)X_{CA} + M_{A1} + KM_{A2})^2 + 4KX_{CA}M_{A2}(1 - K)}}$$

$$F_{A2} = \frac{KM_{A2} - M_{A1} + X_{CA}(1 - K) \pm \sqrt{((1 - K)X_{CA} + M_{A1} + KM_{A2})^2 + 4KX_{CA}M_{A2}(1 - K)}}{M_{A1} + KM_{A2} + X_{CA}(1 - K) \pm \sqrt{((1 - K)X_{CA} + M_{A1} + KM_{A2})^2 + 4KX_{CA}M_{A2}(1 - K)}}$$

Equation S6. F_{A1} and F_{A2} defined in terms of X_{CA}.

In order to easily determine the excess anion at a given concentration, we consider the case where the mole fraction of each anion is equivalent, i.e. $M_{A1} = M_{A2} = 0.5$. Trivially, if it is assumed $X_{CA} = 1$ (i.e. all anions are interacting with that cation location) F_{A1} and F_{A2} equal 0.5 regardless of the choice of K as this would require that all anions in the system interact with that specific cation location. A fairly conservative choice of $X_{CA} = 0.5$ (i.e. an average of 50% of anions are interacting with H^2 over the NMR timescale) and the use of the largest K value observed for H^2 within our experiments (2.63) yields an excess of A_2 from Equations S6 of 23.8% corresponding to a time-weighted composition of anions around H^2 of 38.1% $[NTf_2]^-$ and 61.9% $[Me_2PO_4]^-$. If a larger proportion of anions were interacting with the H^2 position, this excess value would be even smaller, for example, 75% of anions interacting would yield an excess of A_2 of only 11.7%.

References

1. E. Bosch and M. Rosés, *J. Chem. Soc. Faraday Trans.*, 1992, 88, 3541-3546.
2. R. D. Skwierczynski and K. A. Connors, *J. Chem. Soc. Perkin Trans. 2*, 1994, 467-472.
3. A. D. Becke, *J. Chem. Phys.*, 1993, 98, 5648-5652.
4. C. Lee, W. Yang and R. G. Parr, *Phys. Rev. B*, 1988, 37, 785-789.
5. M. J. Frisch, G. W. Trucks, H. B. Schlegel, G. E. Scuseria, M. A. Robb, J. R. Cheeseman, G. Scalmani, V. Barone, B. Mennucci, G. A. Petersson, H. Nakatsuji, M. Caricato, X. Li, H. P. Hratchian, A. F. Izmaylov, J. Bloino, G. Zheng, J. L. Sonnenberg, M. Hada, M. Ehara, K. Toyota, R. Fukuda, J. Hasegawa, M. Ishida, T. Nakajima, Y. Honda, O. Kitao, H. Nakai, T. Vreven, J. A. Montgomery, Jr., J. E. Peralta, F. Ogliaro, M. Bearpark, J. J. Heyd, E. Brothers, K. N. Kudin, V. N. Staroverov, R. Kobayashi, J. Normand, K. Raghayachari, A. Rendell, J. C. Burant, S. S. Iyengar, J. Tomasi, M. Cossi, N. Rega, J. M. Millam, M. Klene, J. E. Knox, J. B. Cross, V. Bakken, C. Adamo, J. Jaramillo, R. Gomperts, R. E. Stratmann, O. Yazyev, A. J. Austin, R. Cammi, C. Pomelli, J. W. Ochterski, R. L. Martin, K. Morokuma, V. G. Zakrewski, G. A. Voth, P. Salvador, J. J. Dannenberg, S. Dapprich, A. D. Daniels, O. Farkas, J. B. Foresman, J. V. Ortiz, J. Cioslowki and D. J. Fox, Gaussian, Inc., Wallingford CT, 2009.
6. S. Grimme, J. Antony, S. Ehrlich and H. Krieg, *J. Chem. Phys.*, 2010, 132, 154104.

7. S. Grimme, S. Ehrlich and L. Goerigk, *J. Comput. Chem.*, 2011, 32, 1456-1465.
8. E. R. Johnson and A. D. Becke, *J. Chem. Phys.*, 2005, 123, 024101.
9. A. D. Becke and E. R. Johnson, *J. Chem. Phys.*, 2005, 123, 154101.
10. A. D. Becke and E. R. Johnson, *J. Chem. Phys.*, 2006, 124, 014104.
11. R. P. Matthews, C. Ashworth, T. Welton and P. A. Hunt, *J. Phys.: Condens. Matter*, 2014, 26, 284112.
12. V. S. Bernales, A. V. Marenich, R. Contreras, C. J. Cramer and D. G. Truhlar, *J. Phys. Chem. B*, 2012, 116, 9122-9129.
13. J. G. Huddleston, A. E. Visser, W. M. Reichert, H. D. Willauer, G. A. Broker and R. D. Rogers, *Green Chem.*, 2001, 3, 156-164.
14. M. A. Ab Rani, A. Brant, L. Crowhurst, A. Dolan, M. Y. Lui, N. H. Hassan, J. P. Hallett, P. A. Hunt, H. Niedermeyer, J. M. Perez-Arlandis, M. Schrems, T. Welton and R. Wilding, *Phys. Chem. Chem. Phys.*, 2011, 13, 16831-16840.
15. T. A. Keith, TK Gristmill Software, Overland Park KS, USA, 13.11.04 edn., 2013.
16. W. Smith and T. R. Forester, *J. Mol. Graphics*, 1996, 14, 136-141.
17. J. N. Canongia Lopes, A. A. H. Pádua and K. Shimizu, *J. Phys. Chem. B*, 2008, 112, 5039-5046.
18. J. N. Canongia Lopes and A. A. H. Pádua, *J. Phys. Chem. B*, 2004, 108, 16893-16898.
19. W. L. Jorgensen, D. S. Maxwell and J. Tirado-Rives, *J. Am. Chem. Soc.*, 1996, 118, 11225-11236.
20. B. D. Rabideau and A. E. Ismail, *Phys. Chem. Chem. Phys.*, 2015, 17, 5767-5775.
21. A. A. Niazi, B. D. Rabideau and A. E. Ismail, *J. Phys. Chem. B*, 2013, 117, 1378-1388.
22. L. Martínez, R. Andrade, E. G. Birgin and J. M. Martínez, *J. Comput. Chem.*, 2009, 30, 2157-2164.
23. M. P. Allen and D. J. Tildesley, *Computer Simulation of Liquids*, Oxford University Press, New York, NY, USA, 1987.
24. W. G. Hoover, *Phys. Rev. A*, 1985, 31, 1695-1697.
25. J.-P. Ryckaert, G. Ciccotti and H. J. C. Berendsen, *J. Comput. Phys.*, 1977, 23, 327-341.
26. W. Smith and T. R. Forester, *Comput. Phys. Commun.*, 1994, 79, 63-77.
27. M. Brehm and B. Kirchner, *J. Chem. Inf. Model.*, 2011, 51, 2007-2023.
28. W. Humphrey, A. Dalke and K. Schulten, *J. Mol. Graphics*, 1996, 14, 33-38.
29. R. S. Payal and S. Balasubramanian, *Phys. Chem. Chem. Phys.*, 2013, 15, 21077-21083.
30. I. Skarmoutsos, T. Welton and P. A. Hunt, *Phys. Chem. Chem. Phys.*, 2014, 16, 3675-3685.
31. R. Lungwitz, V. Strehmel and S. Spange, *New J. Chem.*, 2010, 34, 1135-1140.
32. P. A. Hunt, C. R. Ashworth and R. P. Matthews, *Chem. Soc. Rev.*, 2015, 44, 1257-1288.